
The Recurrent Neural Tangent Kernel

Sina Alemohammad, Zichao Wang, Randall Balestriero, Richard Baraniuk
Rice University
Houston, Texas, USA

Abstract

The study of deep networks (DNs) in the infinite-width limit, via the so-called *neural tangent kernel* (NTK) approach, has provided new insights into the dynamics of learning, generalization, and the impact of initialization. One key DN architecture remains to be kernelized, namely, the recurrent neural network (RNN). In this paper we introduce and study the *Recurrent Neural Tangent Kernel* (RNTK), which sheds new insights into the behavior of overparametrized RNNs, including how different time steps are weighted by the RNTK to form the output under different initialization parameters and nonlinearity choices, and how inputs of different lengths are treated. We demonstrate via a number of experiments that the RNTK offers significant performance gains over other kernels, including standard NTKs across a range of different data sets. A unique benefit of the RNTK is that it is agnostic to the length of the input, in stark contrast to other kernels.

1 Introduction

The overparameterization of modern deep (neural) networks (DNs) has resulted in not only unreasonably good generalization performance on unseen data [7, 29, 30] but also guarantees that gradient descent learning can find the global minimum of their highly nonconvex loss functions [1, 2, 5, 14, 36]. From these successes, a natural question arises: What happens when we take overparameterization to the limit by allowing the width of a DN’s hidden layers to go to infinity? Surprisingly, the behavior of such an (impractical) DN becomes analytically tractable. Indeed, recent work has shown that the training dynamics of (infinite width) DN under gradient flow is captured by a constant kernel called the *Neural Tangent Kernel* (NTK) that evolves according to a linear ordinary differential equation (ODE) [4, 23, 27].

Each different DN architecture and parameter initialization produces a distinct NTK. The original NTK was derived from the Multilayer Perceptron [23] and was soon followed by kernels derived from Convolutional Neural Networks (CNTK) [4, 34], Residual DNs [21], and Graph Convolutional Neural Networks (GNTK) [13].

*In this paper, we extend the NTK concept to the important class of overparametrized Recurrent Neural Networks (RNNs), a fundamental building block for processing sequential data. We show that an RNN in its infinite width limit converges to a kernel that we dub the **Recurrent Neural Tangent Kernel** (RNTK). In addition to being a high performing kernel for various machine learning tasks, analysis of the RNTK provides useful insights into the behavior of RNNs in the overparametrized regime. In this paper, we derive and study the RNTK to answer the following theoretical questions:*

Q: Can the RNTK extract long-term dependencies between two data sequences? RNNs are known to underperform at learning long-term dependencies due to the gradient vanishing or exploding [8]. Attempted ameliorations have included orthogonal weights [3, 18, 24] and gating such as in Long Short-Term Memory (LSTM) [19] and Gated Recurrent Unit (GRU) [11] RNNs. We demonstrate that the RNTK can detect long term dependencies with proper initialization hyperparameters, and

moreover, we show how the dependencies are extracted through time using different hyperparameter choices.

Q: Do the recursive weights of the RNTK reduce its representation power compared to other NTKs? An attractive property of RNNs that is shared by the RNTK is that they can deal with sequences of different length via weight-sharing through time. When the data sequence length is fixed, however, we can (roughly) treat an RNN as a feed-forward network and allow the weights to vary at each time step, presumably resulting in a more powerful model. We prove that allowing the RNN weights to vary over time does not change the space of functions that RNTK learns to represent.

Q: Does the RNTK generalize well? A recent study has revealed that the use of a SVM classifier with the NTK, CNTK, and GNTK kernels outperforms more classical kernel-based classifiers and finite DNs on small data sets (typically less than 5000 training samples) [6, 13]. We show that the RNTK is superior to all of the above kernels, including NTK, CNTK, and GNTK, and finite RNNs for small time series data sets for both classification and regression tasks.

We summarize our contributions as follows:

[C1] We derive the analytical form of the RNTK for an overparametrized RNN at initialization using rectified linear unit (ReLU) and error function (erf) nonlinearities (Section 3.1).

[C2] We prove that the RNTK remains constant during (overparametrized) RNN training and that the dynamics of training are simplified to a set of ODEs (Section 3.2).

[C3] When the input time series are all of equal length, we show that the RNTKs of a weight-tied and weight-untied RNN converge to the same RNTK (Section 3.3).

[C4] Leveraging our analytical formula for the RNTK, we empirically demonstrate how correlations between data at different times are weighted by the function learned by an RNN under different sets of hyper-parameters. We also offer practical suggestions for choosing the RNN hyperparameters for stable information propagation through time (Section 3.4).

[C5] We demonstrate convincingly that the RNTK is eminently practical by showing that it outperforms NTK and a range of classical kernels in exhaustive experiments on time-series classification and regression with both synthetic and 53 real-world data sets (Section 4).

2 Background and Related Work

Notation. We denote $[n] = \{1, \dots, n\}$, and \mathbf{I}_d as identity matrix of size d . $[\mathbf{A}]_{i,j}$ represents the (i, j) -th entry of a matrix and similarly $[\mathbf{a}]_i$ represents the i -th entry of a vector. We use notation $\phi(\cdot) : \mathbb{R} \rightarrow \mathbb{R}$ for the activation function that acts coordinate wise on a vector and ϕ' denotes its derivative. We use rectified linear unit (ReLU) : $\phi(x) = \max(0, x)$ and error function (erf) : $\phi(x) = \frac{2}{\sqrt{\pi}} \int_0^x e^{-z^2} dz$. $\mathcal{N}(\boldsymbol{\mu}, \boldsymbol{\Sigma})$ represents the Gaussian distribution with mean vector $\boldsymbol{\mu}$ and the covariance matrix $\boldsymbol{\Sigma}$.

Recurrent Neural Networks (RNNs). Given an input sequence $\mathbf{x} = \{\mathbf{x}_t\}_{t=1}^T$, $\mathbf{x}_t \in \mathbb{R}^m$, a simple RNN [16] performs the following recursive computation at each layer ℓ and each time step t

$$\mathbf{g}^{(\ell,t)}(\mathbf{x}) = \mathbf{W}^{(\ell)} \mathbf{h}^{(\ell,t-1)}(\mathbf{x}) + \mathbf{U}^{(\ell)} \mathbf{h}^{(\ell-1,t)}(\mathbf{x}) + \mathbf{b}^{(\ell)}, \quad \mathbf{h}^{(\ell,t)}(\mathbf{x}) = \phi\left(\mathbf{g}^{(\ell,t)}(\mathbf{x})\right), \quad (1)$$

where $\mathbf{W}^{(\ell)} \in \mathbb{R}^{n \times n}$, $\mathbf{b}^{(\ell)} \in \mathbb{R}^n$ for $\ell \in [L]$, $\mathbf{U}^{(1)} \in \mathbb{R}^{n \times m}$ and $\mathbf{U}^{(\ell)} \in \mathbb{R}^{n \times n}$ for $\ell \geq 2$ are RNN parameters. $\mathbf{h}^{(\ell,t)}(\mathbf{x})$ is the after-activation (hidden state) and $\mathbf{g}^{(\ell,t)}(\mathbf{x})$ is the pre-activation vector at layer ℓ and time step t . For the input layer $\ell = 0$, we define $\mathbf{h}^{(0,t)}(\mathbf{x}) := \mathbf{x}_t$. $\mathbf{h}^{(\ell,0)}(\mathbf{x})$ is the initial hidden state at layer ℓ which needs to be set to some value beforehand to start the RNN recursive computation. $\phi(\cdot) : \mathbb{R} \rightarrow \mathbb{R}$ is a nonlinear activation function that act element wise on a vector. Let T be the length of the sequence of input data. The output of a L -hidden layer RNN with linear read out layer is achieved via

$$f_{\theta}(\mathbf{x}) = \mathbf{V} \mathbf{h}^{(L,T)}(\mathbf{x}), \quad (2)$$

where $\mathbf{V} \in \mathbb{R}^{d \times n}$. Note that, in 1 and 2, the input \mathbf{x} in parentheses highlights the dependency of these variables on the input. Figure 1 visualizes an RNN unrolled in time.

Neural Tangent Kernel (NTK). Let $f_{\theta}(\mathbf{x}) \in \mathbb{R}^d$ be the output of a DN with parameter set θ . Neural Tangent Kernel is defined as [23]

$$\widehat{\Theta}_s(\mathbf{x}, \mathbf{x}') = \langle \nabla_{\theta_s} f_{\theta_s}(\mathbf{x}), \nabla_{\theta_s} f_{\theta_s}(\mathbf{x}') \rangle, \quad (3)$$

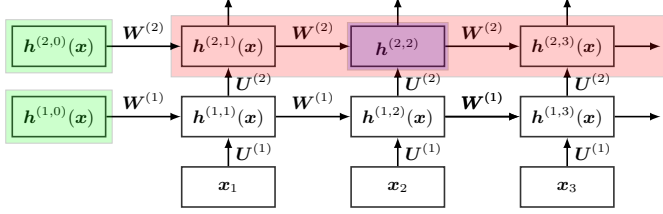


Figure 1: Visualization of an RNN that highlights a cell (purple), a layer (red) and the initial hidden state of each layer (green). (Best viewed in color.)

where f_{θ_s} and θ_s are the network output and parameters during training at time s .¹ Let \mathcal{X} and \mathcal{Y} be the set of training inputs and targets, $\ell(\hat{y}, y) : \mathbb{R}^d \times \mathbb{R}^d \rightarrow \mathbb{R}^+$ be the loss function and $\mathcal{L} = \frac{1}{|\mathcal{X}|} \sum_{(\mathbf{x}, \mathbf{y}) \in \mathcal{X} \times \mathcal{Y}} \ell(f_{\theta_s}(\mathbf{x}), \mathbf{y})$ be the empirical loss. The evolution of parameters θ_s and output of the network f_{θ_s} on test input under gradient flow with learning rate η is formulated as

$$\frac{\partial \theta_s}{\partial s} = -\eta \nabla_{\theta_s} f_{\theta_s}(\mathcal{X})^T \nabla_{f_{\theta_s}(\mathcal{X})} \mathcal{L} \quad (4)$$

$$\frac{\partial f_{\theta_s}(\mathbf{x})}{\partial s} = -\eta \nabla_{\theta_s} f_{\theta_s}(\mathbf{x}) \nabla_{\theta_s} f_{\theta_s}(\mathcal{X})^T \nabla_{f_{\theta_s}(\mathcal{X})} \mathcal{L} = -\eta \hat{\Theta}_s(\mathbf{x}, \mathcal{X}) \nabla_{f_{\theta_s}(\mathcal{X})} \mathcal{L}. \quad (5)$$

Generally, $\hat{\Theta}_s(\mathbf{x}, \mathbf{x}')$, hereafter refereed as empirical NTK, changes overtime during training, making the analysis of training dynamic difficult. In case f_{θ_s} corresponds to a infinite width MLP, [23] showed that $\hat{\Theta}_s(\mathbf{x}, \mathbf{x}')$ converges to a limiting kernel at initialization and stays constant during training, i.e.,

$$\lim_{n \rightarrow \infty} \hat{\Theta}_s(\mathbf{x}, \mathbf{x}') = \lim_{n \rightarrow \infty} \hat{\Theta}_0(\mathbf{x}, \mathbf{x}') := \Theta(\mathbf{x}, \mathbf{x}') \quad \forall s, \quad (6)$$

which is equivalent to replacing the outputs of the DN by its first order Taylor expansion in the parameter space [27]. In case of MSE loss function, training dynamics in 4 and 5 simplifies to a set of linear ODEs, which is the same as training dynamics of kernel ridge regression with respect to NTK when the ridge term goes to zero. A none zero ridge term appears by adding a regularization term $\frac{\lambda^2}{2} \|\theta_s - \theta_0\|_2^2$ to the empirical loss [20].

3 The Recurrent Neural Tangent Kernel

We are now ready to derive the RNTK. We first show the convergence of RNN at initialization to RNTK in the infinite width limit and discuss various insights it enables. We then derive the convergence of RNN after training to RNTK. Finally, we analyze the effect of various hyperparameter choices on RNTK. Proofs of all theorems are available in the Supplementary Material (SM).

3.1 RNTK For Infinite-Width RNN at Initialization

First we specify the following parameter initialization scheme that follows previous work on NTKs [23], which is crucial to our convergence results

$$\mathbf{W}^{(\ell)} = \frac{\sigma_w^\ell}{\sqrt{n}} \mathbf{W}^{(\ell)}, \quad \mathbf{U}^{(1)} = \frac{\sigma_u^1}{\sqrt{m}} \mathbf{U}^{(1)}, \quad \mathbf{U}^{(\ell)} = \frac{\sigma_u^\ell}{\sqrt{n}} \mathbf{U}^{(\ell)} (\ell \geq 2), \quad \mathbf{V} = \frac{\sigma_v}{\sqrt{n}} \mathbf{V}, \quad \mathbf{b}^{(\ell)} = \sigma_b \mathbf{b}^{(\ell)}, \quad (7)$$

where

$$[\mathbf{W}^\ell]_{i,j}, [\mathbf{U}^{(\ell)}]_{i,j}, [\mathbf{V}]_{i,j}, [\mathbf{b}^{(\ell)}]_i \sim \mathcal{N}(0, 1). \quad (8)$$

We refer to (7) and (8) as the *NTK initialization*. The choices of the hyperparameters σ_w , σ_u , σ_v and σ_b can significantly impact RNN performance and we discuss them in detail in Section 3.4. For the initial (at time $t = 0$) hidden state at each layer ℓ , we set $\mathbf{h}^{(\ell,0)}(\mathbf{x})$ an i.i.d copy of $\mathcal{N}(0, \sigma_h)$ [33]. For convenience, we collect all learnable parameters in RNN into $\theta = \text{Vect}[\{\{\mathbf{W}^\ell, \mathbf{U}^\ell, \mathbf{b}^\ell\}_{\ell=1}^L, \mathbf{V}\}]$.

Derivation RNTK at initialization is built upon the correspondence of randomly initialized infinite width neural networks (NNs) to Gaussian Processes (GPs), known as NN-GP. As first shown in [28] for a single layer fully connected neural network under i.i.d. Gaussian initialization of θ , every

¹We use s to denote time since t is used to index time steps of RNN inputs.

coordinate of the output of the NN tends to a GP as the number of neurons at the hidden layer width goes to infinity, with kernel computed as

$$\mathcal{K}(\mathbf{x}, \mathbf{x}') = \mathbb{E}_{\theta \sim \mathcal{N}} [[f_{\theta}(\mathbf{x})]_i \cdot [f_{\theta}(\mathbf{x}')]_i], \quad \forall i \in [d]. \quad (9)$$

Similar to [28], recent works have also linked NNs to GPs for different NN architectures [15, 17, 26, 31, 35], where every pre-activation layers and output of the function tends to GPs in the infinite width limit. In the case of RNNs, each coordinate of the RNN pre-activation $\mathbf{g}^{(\ell,t)}(\mathbf{x})$ converge to a centered GP depending on the inputs and with kernel

$$\Sigma^{(\ell,t,t')}(\mathbf{x}, \mathbf{x}') = \mathbb{E}_{\theta \sim \mathcal{N}} [[\mathbf{g}^{(\ell,t)}(\mathbf{x})]_i \cdot [\mathbf{g}^{(\ell,t')}(\mathbf{x}')]_i] \quad \forall i \in [n]. \quad (10)$$

Also, as per [34], gradients computed in back propagation of random infinite width NNs are also Gaussian distributed. In the case of RNNs, every coordinate of vector $\boldsymbol{\delta}^{(\ell,t)}(\mathbf{x}) := \sqrt{n}(\nabla_{\mathbf{g}^{(\ell,t)}(\mathbf{x})} f_{\theta}(\mathbf{x}))$ converges to a GP with kernel

$$\Pi^{(\ell,t,t')}(\mathbf{x}, \mathbf{x}') = \mathbb{E}_{\theta \sim \mathcal{N}} [[\boldsymbol{\delta}^{(\ell,t)}(\mathbf{x})]_i \cdot [\boldsymbol{\delta}^{(\ell,t')}(\mathbf{x}')]_i] \quad \forall i \in [n]. \quad (11)$$

Both convergences occur independent of the coordinate index i and for possibly different length inputs, i.e., $T \neq T'$. With (10) and (11), we now prove that an infinite-width RNN at initialization converges to the limiting RNTK, formally stated in the theorem below.

Theorem 1 *Let \mathbf{x} and \mathbf{x}' be two sequence of data potentially different lengths T and T' , respectively. Without loss of generality, assume that $T \leq T'$ and let $\tau := T' - T$. The empirical RNTK for an L -layer RNN with NTK initialization converges to the following limiting kernel as $n \rightarrow \infty$*

$$\lim_{n \rightarrow \infty} \widehat{\Theta}_0(\mathbf{x}, \mathbf{x}') = \Theta(\mathbf{x}, \mathbf{x}') = \Theta^{(L,T,T')}(\mathbf{x}, \mathbf{x}') \otimes \mathbf{I}_d, \quad (12)$$

where

$$\Theta^{(L,T,T')}(\mathbf{x}, \mathbf{x}') = \left(\sum_{\ell=1}^L \sum_{t=1}^T (\Pi^{(\ell,t,t+\tau)}(\mathbf{x}, \mathbf{x}') \cdot \Sigma^{(\ell,t,t+\tau)}(\mathbf{x}, \mathbf{x}')) \right) + \mathcal{K}(\mathbf{x}, \mathbf{x}'), \quad (13)$$

and $\Pi^{(\ell,t,t+\tau)}(\mathbf{x}, \mathbf{x}')$, $\Sigma^{(\ell,t,t+\tau)}(\mathbf{x}, \mathbf{x}')$ and $\mathcal{K}(\mathbf{x}, \mathbf{x}')$ are defined in Eqs. 11, 10, and 9, respectively.

Remarks. Theorem 1 holds for all and possibly different lengths of data. Thus we highlight a powerful ability of the RNTK to inherently deal with different length inputs. That is, RNTK can compute the similarity measure $\Theta(\mathbf{x}, \mathbf{x}')$ for inputs with arbitrary and untied lengths without any ad-hoc intervention such as zero padding inputs to the same length. This is different from common kernels such as RBF and polynomial and any currently derived NTKs which have to resort to some flavors of zero padding when dealing with different length inputs. We will demonstrate in Section 4 that RNTK without ad-hoc zero padding offers a significant hedge over other kernels that requires such padding for tasks involving different length inputs.

To visualize Theorem 1, we plot the convergence in the left plot in Figure 2, using as an example a single layer RNN with a pair of simple inputs of different lengths, i.e., $\mathbf{x} = \{1, -1, 1\}$ and $\mathbf{x}' = \{\cos(\alpha), \sin(\alpha)\}$ where $\alpha = [0, 2\pi]$. The plot clearly demonstrates that a sufficiently large hidden state ($n = 1000$) converges to its RNTK ($n = \infty$).

RNTK Example for a Single-Layer RNN. We present a concrete example of Theorem 1 by showing how to recursively compute the RNTK for a single-layer RNN, thus we drop the indices for layers for notational simplicity. *We compute and display the RNTK for a more general, multi-layer RNN in the Supplemental Materials (Section B.3) rather than in the main text due to space limitations.* To compute the RNTK $\Theta^{(T,T')}(\mathbf{x}, \mathbf{x}')$, we need to compute the GP kernels $\Sigma^{(t,t+\tau)}(\mathbf{x}, \mathbf{x}')$ and $\Pi^{(t,t+\tau)}(\mathbf{x}, \mathbf{x}')$. We first define an operator $V_{\phi}[\mathbf{K}]$ given the nonlinearity $\phi(\cdot)$ and a positive semi-definite matrix $\mathbf{K} \in \mathbb{R}^2$

$$V_{\phi}[\mathbf{K}] = \mathbb{E}[\phi(\mathbf{z}_1) \cdot \phi(\mathbf{z}_2)], \quad (\mathbf{z}_1, \mathbf{z}_2) \sim \mathcal{N}(0, \mathbf{K}). \quad (14)$$

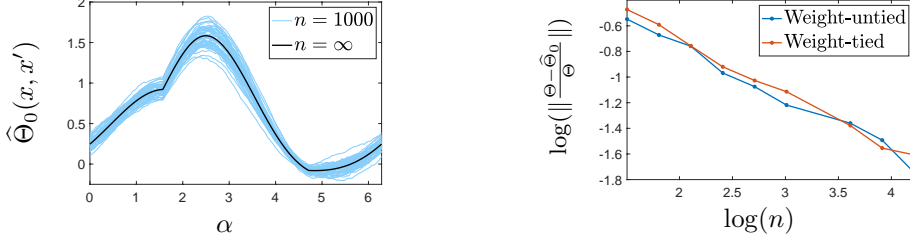


Figure 2: Empirical demonstration of a wide, single layer RNN converging to its limiting RNTK. **Left plot** demonstrates convergence for a pair of different length inputs, i.e., $\mathbf{x} = \{1, -1, 1\}$ and $\mathbf{x}' = \{\cos(\alpha), \sin(\alpha)\}$, with varying $\alpha = [0, 2\pi]$. y-axis shows the RNTK values. **Right plot** demonstrates convergence of weight-tied and weight-untied RNNs to the same limiting RNTK with increasing width (x-axis). y-axis is the average of log-normalized error between the empirical RNTK computed using finite RNNs and the theoretical RNTK.

Following [12, 28] (and more details in SM B.1), we obtain the recursive analytical formula for the GP kernel $\Sigma^{(t, t+\tau)}(\mathbf{x}, \mathbf{x}')$ for a single layer RNN as

$$\Sigma^{(1,1)}(\mathbf{x}, \mathbf{x}') = \sigma_w^2 \sigma_h^2 1_{(\mathbf{x}=\mathbf{x}')} + \frac{\sigma_u^2}{m} \langle \mathbf{x}_1, \mathbf{x}'_1 \rangle + \sigma_b^2 \quad (15)$$

$$\Sigma^{(t, t')}(\mathbf{x}, \mathbf{x}') = \sigma_w^2 V_\phi[\mathbf{K}^{(t, t')}(\mathbf{x}, \mathbf{x}')] + \frac{\sigma_u^2}{m} \langle \mathbf{x}_t, \mathbf{x}'_{t'} \rangle + \sigma_b^2 \quad (16)$$

$$\mathcal{K}(\mathbf{x}, \mathbf{x}') = \sigma_v^2 V_\phi[\mathbf{K}^{(T+1, T'+1)}(\mathbf{x}, \mathbf{x}')], \quad (17)$$

where

$$\mathbf{K}^{(t, t')}(\mathbf{x}, \mathbf{x}') = \begin{bmatrix} \Sigma^{(t-1, t-1)}(\mathbf{x}, \mathbf{x}) & \Sigma^{(t-1, t'-1)}(\mathbf{x}, \mathbf{x}') \\ \Sigma^{(t-1, t'-1)}(\mathbf{x}, \mathbf{x}') & \Sigma^{(t'-1, t'-1)}(\mathbf{x}', \mathbf{x}') \end{bmatrix}. \quad (18)$$

Similarly, we obtain the recursive analytical formula for the GP kernel $\Pi^{(t, t+\tau)}(\mathbf{x}, \mathbf{x}')$ as

$$\Pi^{(T, T')}(\mathbf{x}, \mathbf{x}') = \sigma_v^2 V_{\phi'}[\mathbf{K}^{(T+1, T'+1)}(\mathbf{x}, \mathbf{x}')] \quad (19)$$

$$\Pi^{(t, t+u)}(\mathbf{x}, \mathbf{x}') = \sigma_w^2 V_{\phi'}[\mathbf{K}^{(t+1, t'+1)}(\mathbf{x}, \mathbf{x}')] \Pi^{(t+1, t'+1+u)}(\mathbf{x}, \mathbf{x}') \quad t \in [T-1] \quad (20)$$

$$\Pi^{(t, t')}(\mathbf{x}, \mathbf{x}') = 0 \quad t' - t \neq \tau \quad (21)$$

When $\phi = \text{ReLU}$ and $\phi = \text{erf}$ is used, analytical expression exists for $V_\phi[\mathbf{K}]$, $V_{\phi'}[\mathbf{K}]$ which leads to an analytical expression for RNTK. See SM B.5 for an explicit formula. This allows fast and point wise evaluation of kernel on the input, otherwise it can be estimated numerically using Monte Carlo method as proposed in [31] for other nonlinearities.

3.2 RNTK For Infinite-Width RNN After Training

We show that an infinitely wide RNN, even *after* training with gradient descent, also converges to a limiting kernel which coincides with the RNTK that the RNN at initialization converges to. This result provides insights into the dynamics of training RNNs which complements prior work on RNN stability and convergence during training [2]. We formalize the convergence result of a trained RNN in the theorem below.

Theorem 2 *Let n be the number of units at each layer. Assume that $\Theta(\mathcal{X}, \mathcal{X})$ is positive definite on \mathcal{X} such that $\lambda_{\min}(\Theta(\mathcal{X}, \mathcal{X})) > 0$. Let $\eta^* := 2(\lambda_{\min}(\Theta(\mathcal{X}, \mathcal{X})) + \lambda_{\max}(\Theta(\mathcal{X}, \mathcal{X})))^{-1}$. For an L -layer RNN with NTK initialization (7 and 8) trained under gradient flow with $\eta < \eta^*$, with high probability, we have*

$$\sup_s \|\hat{\Theta}_s(\mathcal{X}, \mathcal{X}) - \hat{\Theta}_0(\mathcal{X}, \mathcal{X})\| = \mathcal{O}\left(\frac{1}{\sqrt{n}}\right) \quad (22)$$

Remarks. Theorem 2 essentially states that the training dynamics of an RNN in the infinite width limit stated in 4 and 5 is governed by the RNTK derived from the RNN at its initialization and stays the same during training. Intuitively, this is due to the minimal number of required updates in the weights to fit the data under the initialization from 7 and 8.

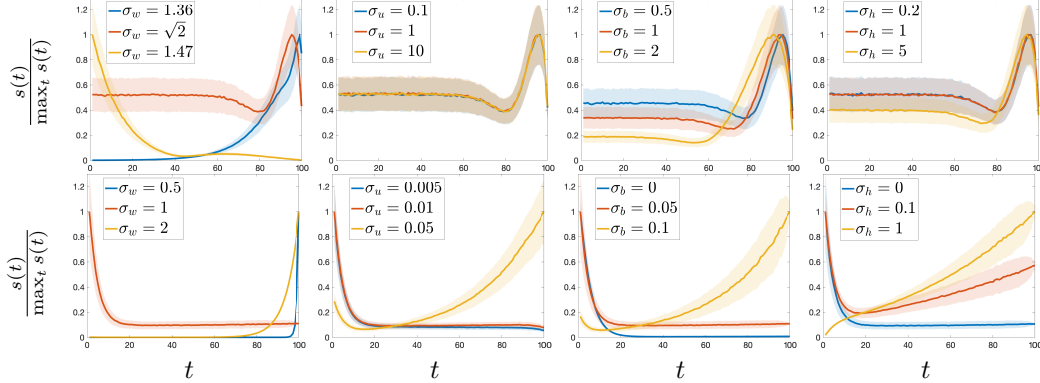


Figure 3: Demonstration of the sensitivity analysis of RNTK for ReLU (top row) and erf (bottom row) nonlinearities, for various weight noise hyperparameters and for inputs at each time step (x-axis). This analysis suggests that ReLU is more stable than erf for a range of RNTK hyperparameters.

3.3 RNTK for Infinite-Width RNN Without Weight Sharing

We show that an RNN without weight sharing (untied weights) has similar behavior to RNN with weight sharing (tied weights) in the infinite width limit. First, recall that it is a common practice to use weight-tied RNNs, i.e., in a given layer ℓ , the weights $\mathbf{W}^{(\ell)}$, $\mathbf{U}^{(\ell)}$ and $\mathbf{b}^{(\ell)}$ are the same across all time steps t . We thus omit the t index in the preceding presentations. This practice allows to save memory and reduce the number of learnable parameters. We now demonstrate that when using such untied-weights, as opposed to the weight-tied settings from the above analysis with Theorem 1, the RNTK formula remains unchanged.

Theorem 3 *For inputs of the same length, an RNN with untied weights converges to the same RNTK as an RNN with tied weights in the infinite width ($n \rightarrow \infty$) regime.*

Remarks. Theorem 3 implies that weight-tied and weight-untied RNNs have similar behaviors in the infinite width limit and, suggesting that existing results on the simpler, weight-untied RNN setting may be applicable for the more general, weight-tied RNN. We visualize Theorem 3 in the plot on the right side of Figure 2 and show that both weight-tied and weight-untied RNNs converge to RNTK with increasing hidden layer size n and the convergence speeds are similar. Notice that the convergence to a unique kernel from weight tied and untied models has been also discovered in the MLP realm [35] from the NN-GP kernel study, and when studying convolutional layers, where tiedness comes from the convolution operator [31].

3.4 Interpretability of the RNTK’s Variance Parameters and Nonlinearity

The class of functions that an overparametrized RNN can learn is determined by its RNTK, which is influenced by RNN configurations, i.e., weight variances $\mathcal{S} = \{\sigma_w, \sigma_u, \sigma_b, \sigma_h\}^2$ and nonlinearity. To inspect the effects of those hyperparameters, we introduce a novel method and propose to compute the *gradient* of RNTK of two sequence of inputs \mathbf{x} and \mathbf{x}' with respect to \mathbf{x}_t defined as:

$$s(t) = \|\nabla_{\mathbf{x}_t} \Theta(\mathbf{x}, \mathbf{x}')\|_2, \quad (23)$$

which is an indicator of how RNTK is sensitive to data at time t , i.e., \mathbf{x}_t , in presence of another sequence of data \mathbf{x}' . Intuitively, when $s(t)$ is too big, it indicates that RNTK is overly sensitive to the input at time t which corresponds to gradient explosion. Similarly, when $s(t)$ is overly small, it indicates that RNTK has forgotten data, a consequence of gradient vanishing. Thus, $s(t)$ provides a tool for us to study how RNTK responds differently to different initialization and nonlinearities. Ideally, we would like $s(t)$ to remain stable for all t for RNTK to be stable.

We demonstrate the normalized $s(t)/\max_t s(t)$ in Figure 3 for two data of the same length $T = 100$, with $s(t)$ derived numerically for $\mathbf{x}_t, \mathbf{x}'_t \sim \mathcal{N}(0, 1)$. Each of plots is shown for change of parameter in $\mathcal{S}_{\text{ReLU}} = \{\sqrt{2}, 1, 0, 0\}$ for $\phi = \text{ReLU}$ and $\mathcal{S}_{\text{erf}} = \{1, 0.01, 0.05, 0\}$ for $\phi = \text{erf}$.

²From the formulas we emphasize that σ_v merely scales the RNTK and does not change its overall behaviour.

Table 1: Summary of time series classification results on 53 real-world data sets. RNTK outperforms all other kernels that we consider as well as several trained RNNs, including GRU, across all metrics.

	RNTK	NTK	RBF	Polynomial	Gaussian RNN	Identity RNN	GRU
Acc. mean	80.44%	78.29%	78.46%	78.68%	57.34%	64.68%	70.58%
Acc. std	16.08%	16.82%	16.76%	16.58%	26.29%	18.11%	22.70%
Rank Mean	2.35	2.96	2.90	3.60	5.81	5.16	4.15

From visual inspection, we first observe that both ReLU and erf show a stable behaviour around the proposed hyperparameters $\mathcal{S}_{\text{ReLU}}$ and \mathcal{S}_{erf} . Changes in each of the weight variance exhibit a wide range of behaviour in $s(t)$, in which ReLU is more robust to those changes than erf. We also observe that σ_w has a major influence on $s(t)$. For ReLU, small decrease (increase) in σ_w can lead to over sensitivity of RNTK to data at the last (first) times steps, whereas for erf, any changes in σ_w leads to over sensitivity to the last time steps.

Another notable observation is the importance of σ_h where usually it is set to zero for RNNs. In [33] the authors showed that a non-zero σ_h acts as a regularization that improves the performance of RNN with ReLU nonlinearity. From the sensitivity perspective, this results in reducing the importance of the first time steps. We also see the same behaviour in erf, but with stronger changes as σ_h increases.

This sensitivity analysis provides a practical tool for RNTK hyperparameter tuning. Although RNTK setting is different from the finite RNN setting used in practice, such analysis is potentially useful for hyperparameter tuning in practical RNNs. We leave the investigation of the utility of the sensitivity analysis for practical, finite width RNNs as a future work.

4 Experiments

We now empirically validate the performance of the RNTK compared to classic kernels and trained RNNs on both classification and regression tasks. We compare all methods on a large collection of time series data sets and carefully designed experiment to highlight the properties of RNTK with varying length inputs.

Time Series Classification. The first set of experiment deals with time series inputs with the same length for each data set. We perform experiments on selected data sets from the UCR time-series classification data repository [22]. We restrict ourselves to data sets with less than 1000 training samples and less than 1000 time steps to prevent the complexity overhead of kernel methods, resulting in 53 data sets in total. We compare ReLU RNTK with other kernels including Radial Basis Kernel (RBF), polynomial kernel and ReLU NTK [23], as well as finite RNNs with Gaussian, identity [25] initialization and GRU [11]. For different kernels we train a C-SVM [10] classifier and for finite RNNs we use gradient descent for training. For model hyperparameter tuning, we used 10-fold validation. Details on the data sets and experimental setup are available in the SM A.1.

We report a summary of the classification results over all dataset in Table 1. Detailed results on each of the 53 data sets are available in the SM A.2. We see RNTK outperforms standard kernels as well as NTK and trained RNNs. In addition, the standard deviation of the average accuracy that RNTK achieves is lower, which motivates the use of RNTK as a go-to kernel method for time-series classification. We also see that RNNs do not perform well in this experiment. A possible explanation is that RNNs are much more sensitive to hyperparameters for training [32] and rely on much larger data sets than those considered in this experiment to prevent over fitting. In addition, all other kernels (NTK, RBF and polynomial) do not model the time-serie structure of the data as opposed to RNTK which naturally captures the recurrent behavior of RNNs.

The above results highlights RNTK’s practical utility in providing a state-of-the-art kernel for time-series classification tasks. We now move to a more specific application for which one observes data of varying lengths, a regime RNTK is naturally able to handle.

Time Series Regression. We now propose to test the performance of RNTK on varying length time series including both synthetic data and real data. We compare RNTK to RBF, polynomial and NTK with zero padding.

For the synthetic data, we simulate a sinusoidal signal of one period with 1000 samples and add Gaussian noise where the noise level $\sigma_n = 0.05$. From this fixed signal, we extract $n_{\text{train}} = 20$

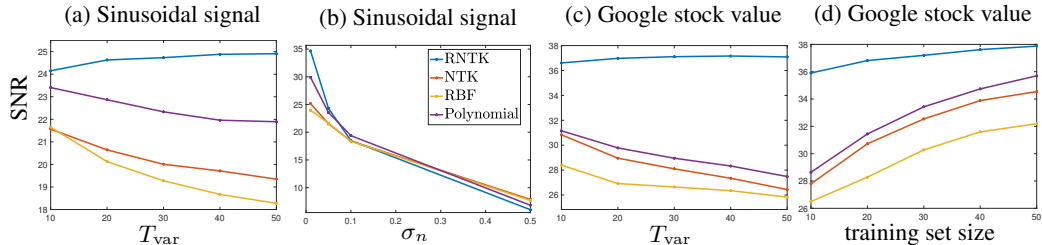


Figure 4: Performance of the RNTK on two data sets comparing to three other kernels with varying input lengths (Figure 4a and 4c), varying input noise levels (Figure 4b) and varying training set size (Figure 4d). We report the average SNR by repeating each experiment 1000 times. RNTK clearly outperforms all other kernels under consideration. Figure 4b suggests that the RNTK is best when input noise level is low.

segments with random length in the range of $[T_{\text{fixed}}, T_{\text{fixed}} + T_{\text{var}}]$ with $T_{\text{fixed}} = 10$. The target of the regression task is the next bin of the randomly long extracted window. The regression method is the standard kernel ridge regression. The test set is made of $n_{\text{test}} = 5000$ obtained from other randomly extracted segments, again with varying length. For the real data, we use 975 days of Google stock value between the years 2014 and 2018. Similar to the setup above, we extract n_{train} segments of varying length as in the above case from the first 700 days and test on 500 other segments in the remaining days.

We report the prediction signal-to-noise ratio (SNR) for both dataset in Figures 4a and 4c for different values of T_{var} . We also vary the noise standard deviation and training size for fixed $T_{\text{var}} = 10$ in Figures 4b and 4d. From Figures 4a and 4b it is clear that RNTK, tanks to its inherent ability to deal with varying length inputs, offers remarkable performance gains compares to other kernels in all situations, and this gap increases with increasing length variation T_{var} between inputs. From Figure 4d, we see that RNTK is able to maintain its performance even when the size of the training set is small, whereas the performances of all other kernels drop significantly with decreasing training set size. Lastly, from Figure 4c, we see that the noise sensitivity is roughly the same for all models but becomes more important for RNTK with large σ_n . One possible reason is that, per the sensitivity analysis (Section 3.4 and Figure 3), RNTK tends to weigh inputs at different time steps differently, thus putting different weights on noises at different time steps and making the overall RNTK prediction more sensitive to increasing noise levels. From this experiment, we emphasize that RNTK offers distinctive advantages over NTKs and other kernel methods for varying length time-series inputs.

5 Conclusions

In this paper, we have derived the Recurrent Neural Tangent Kernel (RNTK) based on the class of simple Recurrent Neural Networks (RNNs). We have shown that an infinite-width RNNs at initialization, after training, and without weight-sharing all converge to the same limiting RNTK. Such a convergence provides new insights into the behavior of infinite-width RNNs, including how they process different length inputs, their training dynamics and the sensitivity of their output at every time step to different nonlinearities and initialization. We have also highlighted the RNTK’s practical utility by demonstrating its superior performance on time series regression and classification tasks compared to other kernel methods and trained RNNs. There are many avenues for future research, including developing RNTKs for gated RNNs such as LSTM [19] and investigating which of our insights extend to finite RNNs.

6 Broader Impacts

RNNs were proposed to model sequence data and has found many real world application up to now, especially in language processing in which its social impacts is apparent. We hope that our theoretical work on RNNs from NTK perspective opens a new gate on addressing unknown properties of RNNs to train, or even build, better models. It also will be of use to practitioner and researchers studying RNN in general regardless of the data and task at hand.

References

- [1] Zeyuan Allen-Zhu, Yuanzhi Li, and Yingyu Liang. Learning and generalization in overparameterized neural networks, going beyond two layers. In *Proc. Adv. Neural Inf. Process. Syst. (NeurIPS)*, pages 6155–6166, 2019.
- [2] Zeyuan Allen-Zhu, Yuanzhi Li, and Zhao Song. On the convergence rate of training recurrent neural networks. In H. Wallach, H. Larochelle, A. Beygelzimer, F. d'Alché-Buc, E. Fox, and R. Garnett, editors, *Proc. Adv. Neural Inf. Process. Syst. (NeurIPS)*, pages 6676–6688. Curran Associates, Inc., 2019.
- [3] Martin Arjovsky, Amar Shah, and Yoshua Bengio. Unitary evolution recurrent neural networks. In *Proc. Intl. Conf. Mach. Learn. (ICML)*, pages 1120–1128, 2016.
- [4] Sanjeev Arora, Simon S Du, Wei Hu, Zhiyuan Li, Ruslan Salakhutdinov, and Ruosong Wang. On exact computation with an infinitely wide neural net. *arXiv preprint arXiv:1904.11955*, 2019.
- [5] Sanjeev Arora, Simon S Du, Wei Hu, Zhiyuan Li, and Ruosong Wang. Fine-grained analysis of optimization and generalization for overparameterized two-layer neural networks. *arXiv preprint arXiv:1901.08584*, 2019.
- [6] Sanjeev Arora, Simon S. Du, Zhiyuan Li, Ruslan Salakhutdinov, Ruosong Wang, and Dingli Yu. Harnessing the power of infinitely wide deep nets on small-data tasks. In *Proc. Int. Conf. Learn. Representations (ICLR)*, 2020.
- [7] Mikhail Belkin, Daniel Hsu, Siyuan Ma, and Soumik Mandal. Reconciling modern machine-learning practice and the classical bias–variance trade-off. *Proc. Nat. Acad. Sci.*, 116(32):15849–15854, 2019.
- [8] Y. Bengio, P. Simard, and P. Frasconi. Learning long-term dependencies with gradient descent is difficult. *IEEE Trans. Neural Networks*, 5(2):157–166, 1994.
- [9] Erwin Bolthausen. An iterative construction of solutions of the tap equations for the sherrington–kirkpatrick model. *Commun. in Math. Phys.*, 325(1):333–366, Dec 2013.
- [10] Chih-Chung Chang and Chih-Jen Lin. LIBSVM: A library for support vector machines. *ACM Transactions on Intelligent Systems and Technology*, 2:27:1–27:27, 2011. Software available at <http://www.csie.ntu.edu.tw/~cjlin/libsvm>.
- [11] K. Cho, B. van Merriënboer, C. Gulcehre, D. Bahdanau, F. Bougares, H. Schwenk, and Y. Bengio. Learning phrase representations using rnn encoder–decoder for statistical machine translation. In *Proc. Conf. Empirical Methods Natural Language Process. (EMNLP)*, pages 1724–1734, October 2014.
- [12] Youngmin Cho and Lawrence K. Saul. Kernel methods for deep learning. In *Proc. Adv. Neural Inf. Process. Syst. (NeurIPS)*, pages 342–350. 2009.
- [13] Simon S Du, Kangcheng Hou, Russ R Salakhutdinov, Barnabas Poczos, Ruosong Wang, and Keyulu Xu. Graph neural tangent kernel: Fusing graph neural networks with graph kernels. In *Proc. Adv. Neural Inf. Process. Syst. (NeurIPS)*, pages 5724–5734, 2019.
- [14] Simon S. Du, Jason D. Lee, Haochuan Li, Liwei Wang, and Xiyu Zhai. Gradient descent finds global minima of deep neural networks, 2018.
- [15] David Duvenaud, Oren Rippel, Ryan P. Adams, and Zoubin Ghahramani. Avoiding pathologies in very deep networks, 2014.
- [16] J. L. Elman. Finding structure in time. *Cogn. Sci.*, 14:179–211, 1990.
- [17] Adria Garriga-Alonso, Carl Edward Rasmussen, and Laurence Aitchison. Deep convolutional networks as shallow gaussian processes, 2018.
- [18] Mikael Henaff, Arthur Szlam, and Yann LeCun. Recurrent orthogonal networks and long-memory tasks. *arXiv preprint arXiv:1602.06662*, 2016.
- [19] Sepp Hochreiter and Jürgen Schmidhuber. Long short-term memory. *Neural computation*, 9(8):1735–1780, 1997.
- [20] Wei Hu, Zhiyuan Li, and Dingli Yu. Simple and effective regularization methods for training on noisily labeled data with generalization guarantee, 2019.
- [21] Kaixuan Huang, Yuqing Wang, Molei Tao, and Tuo Zhao. Why do deep residual networks generalize better than deep feedforward networks? – a neural tangent kernel perspective, 2020.
- [22] P.G. Irving and J.P. Meyer. The ucr time series archive. *IEEE/CAA J. Automatica Sinica*, 6(6):1293–1305, Nov 2019.
- [23] Arthur Jacot, Franck Gabriel, and Clément Hongler. Neural tangent kernel: Convergence and generalization in neural networks. In *Proc. Adv. Neural Inf. Process. Syst. (NeurIPS)*, pages 8571–8580, 2018.
- [24] Li Jing, Yichen Shen, Tena Dubcek, John Peurifoy, Scott Skirlo, Yann LeCun, Max Tegmark, and Marin Soljačić. Tunable efficient unitary neural networks (eunn) and their application to rnns. In *Proc. Intl. Conf. Mach. Learn. (ICML)*, pages 1733–1741. JMLR. org, 2017.

- [25] Q. V. Le, N. Jaitly, and G. E. Hinton. A simple way to initialize recurrent networks of rectified linear units. *ArXiv e-prints*, 1504.00941, Apr. 2015.
- [26] Jaehoon Lee, Yasaman Bahri, Roman Novak, Samuel S Schoenholz, Jeffrey Pennington, and Jascha Sohl-Dickstein. Deep neural networks as gaussian processes. *arXiv preprint arXiv:1711.00165*, 2017.
- [27] Jaehoon Lee, Lechao Xiao, Samuel S. Schoenholz, Yasaman Bahri, Roman Novak, Jascha Sohl-Dickstein, and Jeffrey Pennington. Wide neural networks of any depth evolve as linear models under gradient descent, 2019.
- [28] Radford M Neal. Priors for infinite networks. pages 29–53, 1996.
- [29] Behnam Neyshabur, Zhiyuan Li, Srinadh Bhojanapalli, Yann LeCun, and Nathan Srebro. The role of over-parametrization in generalization of neural networks. In *Proc. Int. Conf. Learn. Representations (ICLR)*, 2019.
- [30] Roman Novak, Yasaman Bahri, Dan Abolafia, Jeffrey Pennington, and Jascha Sohl-dickstein. Sensitivity and generalization in neural networks: an empirical study. 2018.
- [31] Roman Novak, Lechao Xiao, Jaehoon Lee, Yasaman Bahri, Greg Yang, Jiri Hron, Daniel A. Abolafia, Jeffrey Pennington, and Jascha Sohl-Dickstein. Bayesian deep convolutional networks with many channels are gaussian processes, 2018.
- [32] R. Pascanu, T. Mikolov, and Y. Bengio. On the difficulty of training recurrent neural networks. In *Proc. Int. Conf. Mach. Learn. (ICML)*, pages 1310–1318, Jun. 2013.
- [33] Zichao Wang, Randall Balestriero, and Richard Baraniuk. A MAX-AFFINE SPLINE PERSPECTIVE OF RECURRENT NEURAL NETWORKS. In *Proc. Int. Conf. Learn. Representations (ICLR)*, 2019.
- [34] Greg Yang. Scaling limits of wide neural networks with weight sharing: Gaussian process behavior, gradient independence, and neural tangent kernel derivation. *arXiv preprint arXiv:1902.04760*, 2019.
- [35] Greg Yang. Tensor programs i: Wide feedforward or recurrent neural networks of any architecture are gaussian processes. *arXiv preprint arXiv:1910.12478*, 2019.
- [36] Difan Zou, Yuan Cao, Dongruo Zhou, and Quanquan Gu. Stochastic gradient descent optimizes over-parameterized deep relu networks. *arXiv preprint arXiv:1811.08888*, 2018.

A Experiment Details

A.1 Time series classification

Kernel methods settings. We used RNTK, RBF, polynomial and NTK [23]. For data pre-processing, we only normalized the norm of each \mathbf{x} to 1. For training we used C-SVM in LIBSVM library [10] and for hyperparameter selection we performed 10-fold validation for splitting the training data into 90% training set and 10% validation test. We then choose the best performing set of hyperparameters on all the validation sets, retrain the models with the best set of hyperparameters on the entire training data and finally report the performance on the unseen test data. The performance of all kernels on each data set is shown in table 2.

For C-SVM we chose the cost function value

$$C \in \{0.01, 0.1, 1, 10, 100\} \quad (24)$$

and for each kernel we used the following hyperparametr sets

- RNTK: We only used single layer RNTK, we $\phi = \text{ReLU}$ and the following hyperparametr sets for the variances:

$$\sigma_w \in \{1.34, 1.35, 1.36, 1.37, 1.38, 1.39, 1.40, 1.41, 1.42, \sqrt{2}, 1.43, 1.44, 1.45, 1.46, 1.47\} \quad (25)$$

$$\sigma_u = 1 \quad (26)$$

$$\sigma_b \in \{0, 0.01, 0.05, 0.1, 0.2, 0.3, 0.4, 0.5, 0.7, 0.9, 1, 2\} \quad (27)$$

$$\sigma_h \in \{0, 0.01, 0.1, 0.5, 1\} \quad (28)$$

$$(29)$$

- NTK: The formula for NTK of L -layer MLP [23] for $\mathbf{x}, \mathbf{x}' \in \mathbb{R}^m$ is:

$$\Sigma^{(1)} = \frac{\sigma_w^2}{m} \langle \mathbf{x}, \mathbf{x}' \rangle + \sigma_b^2 \quad (30)$$

$$\Sigma^{(\ell)}(\mathbf{x}, \mathbf{x}') = \sigma_w^2 \text{V}_\phi[K^{(\ell)}(\mathbf{x}, \mathbf{x}')] + \sigma_b^2 \quad \ell \in [L] \quad (31)$$

$$\dot{\Sigma}^{(\ell)}(\mathbf{x}, \mathbf{x}') = \sigma_w^2 \text{V}_{\phi'}[K^{(\ell+1)}(\mathbf{x}, \mathbf{x}')] \quad \ell \in [L] \quad (32)$$

$$\mathbf{K}^{(\ell)}(\mathbf{x}, \mathbf{x}') = \begin{bmatrix} \Sigma^{(\ell-1)}(\mathbf{x}, \mathbf{x}) & \Sigma^{(\ell-1)}(\mathbf{x}, \mathbf{x}') \\ \Sigma^{(\ell-1)}(\mathbf{x}, \mathbf{x}') & \Sigma^{(\ell-1)}(\mathbf{x}', \mathbf{x}') \end{bmatrix} \quad (33)$$

$$\mathcal{K}(\mathbf{x}, \mathbf{x}') = \sigma_v^2 \text{V}_\phi[K^{(L+1)}(\mathbf{x}, \mathbf{x}')] \quad (34)$$

$$k_{\text{NTK}} = \sum_{\ell=1}^L \left(\Sigma^{(\ell)}(\mathbf{x}, \mathbf{x}') \prod_{\ell'=\ell}^L \dot{\Sigma}^{(\ell')}(\mathbf{x}, \mathbf{x}') \right) + \mathcal{K}(\mathbf{x}, \mathbf{x}') \quad (35)$$

and we used the following hyperparamters

$$L \in [10] \quad (36)$$

$$\sigma_w \in \{0.5, 1, \sqrt{2}, 2, 2.5, 3\} \quad (37)$$

$$\sigma_b \in \{0, 0.01, 0.1, 0.2, 0.5, 0.8, 1, 2, 5\} \quad (38)$$

- RBF:

$$k_{\text{RBF}}(\mathbf{x}, \mathbf{x}') = e^{(-\alpha \|\mathbf{x} - \mathbf{x}'\|_2^2)} \quad (39)$$

$$\alpha \in \{0.01, 0.05, 0.1, 0.2, 0.5, 0.6, 0.7, 0.8, 1, 2, 3, 4, 5, 10, 20, 30, 40, 100\} \quad (40)$$

- Polynomial:

$$k_{\text{Polynomial}}(\mathbf{x}, \mathbf{x}') = (r + \langle \mathbf{x}, \mathbf{x}' \rangle)^d \quad (41)$$

$$d \in [5] \quad (42)$$

$$r \in \{0, 0.1, 0.2, 0.5, 1, 2\} \quad (43)$$

Finite-width RNN settings. We used 3 different RNNs. The first is a ReLU RNN with Gaussian initialization with the same NTK initialization scheme, where parameter variances are $\sigma_w = \sigma_v = \sqrt{2}$, $\sigma_u = 1$ and $\sigma_b = 0$. The second is a ReLU RNN with identity initialization following [25]. The third is a GRU [11] with uniform initialization. All models are trained with RMSProp algorithm for 200 epochs. Early stopping is implemented when the validation set accuracy does not improve for 5 consecutive epochs.

We perform standard 5-fold cross validation. For each RNN architecture we used hyperparamters of number of layer, number of hidden units and learning rate as

$$L \in \{1, 2\} \quad (44)$$

$$n \in \{50, 100, 200, 500\} \quad (45)$$

$$\eta \in \{0.01, 0.001, 0.0001, 0.00001\} \quad (46)$$

Table 2: Performance of each model on 53 time series data set from UCR time-series classification data repository [22].

Dataset	RNTK	NTK	RBF	POLY	Gaussian RNN	Identity RNN	GRU
Strawberry	98.38	97.57	97.03	96.76	94.32	75.4	91.62
ProximalPhalanxOutlineCorrect	89	87.97	87.29	86.94	82.81	74.57	86.94
PowerCons	97.22	97.22	96.67	91.67	96.11	95	99.44
Ham	70.48	71.63	66.67	71.43	53.33	60	60.95
SmallKitchenAppliances	67.47	38.4	40.27	37.87	60.22	76	71.46
ScreenType	41.6	43.2	43.47	38.4	40	41.06	36.26
MiddlePhalanxOutlineCorrect	57.14	57.14	48.7	64.29	76.28	57.04	74.57
RefrigerationDevices	46.93	37.07	36.53	41.07	36	50.93	46.66
Yoga	84.93	84.63	84.63	84.87	46.43	76.66	61.83
Computers	59.2	55.2	58.8	56.4	53.2	55.2	58.8
ECG5000	93.76	94.04	93.69	93.96	88.4	93.15	93.26
Fish	90.29	84	85.71	88	28	38.28	24
UWaveGestureLibraryX	79.59	78.7	78.48	65.83	55.97	75.34	73.64
UWaveGestureLibraryY	71.56	70.63	70.35	70.32	44.5	65.18	65.38
UWaveGestureLibraryZ	73.95	73.87	72.89	71.94	43.29	67.81	70.32
StarLightCurves	95.94	96.19	94.62	94.44	82.13	86.81	96.15
CricketX	60.51	59.49	62.05	62.56	8.46	63.58	26.41
CricketY	63.85	58.97	60.51	59.74	15.89	59.23	36.15
CricketZ	60.26	59.23	62.05	59.23	8.46	57.94	41.28
DistalPhalanxOutlineCorrect	77.54	77.54	75.36	73.91	69.92	69.56	75
Worms	57.14	50.65	55.84	50.65	35.06	49.35	41.55
SyntheticControl	98.67	96.67	98	97.67	92.66	97.66	99
Herring	56.65	59.38	59.38	59.38	23.28	59.37	59.37
MedicalImages	74.47	73.29	75.26	74.61	48.15	64.86	69.07
SwedishLeaf	90.56	91.04	91.36	90.72	59.2	45.92	91.04
ChlorineConcentration	90.76	77.27	86.35	91.54	65.99	55.75	61.14
SmoothSubspace	96	87.33	92	86.67	94	95.33	92.66
TwoPatterns	94.25	90.45	91.25	93.88	99.7	99.9	100
Faceall	74.14	83.33	83.25	82.43	53.66	70.53	70.65
DistalPhalanxTW	66.19	69.78	66.91	67.37	67.62	64.74	69.06
MiddlePhalanxTW	57.79	61.04	59.74	60.39	58.44	58.44	59.09
FacesUCR	81.66	80.2	80.34	82.98	53.21	75.26	79.46
OliveOil	90	86.67	86.67	83.33	66.66	40	40
UMD	91.67	92.36	97.22	90.97	44.44	71.52	100
nsectEPGRegularTrain	99.6	99.2	99.6	96.79	100	100	98.39
Meat	93.33	93.33	93.33	93.33	0.55	55	33.33
Lightning2	78.69	73.77	70.49	68.85	45.9	70.49	67.21
Lightning7	61.64	60.27	63.01	60.27	23.28	69.86	76.71
Car	83.33	78.83	80	80	23.33	58.33	26.66
GunPoint	98	95.33	95.33	94	82	74.66	80.66
Arrowhead	80.57	83.43	80.57	74.86	48	56	37.71
Coffee	100	100	92.86	92.86	100	42.85	57.14
Trace	96	81	76	76	70	71	100
ECG200	93	89	89	86	86	72	76
plane	98.1	96.19	97.14	97.14	96.19	84.76	96.19
GunPointOldVersusYoung	98.73	97.46	98.73	94.6	53.96	52.38	98.41
GunPointMaleVersusFemale	99.05	99.68	99.37	99.68	68.67	52.53	99.68
GunPointAgeSpan	96.52	94.62	95.89	93.99	47.78	47.78	95.56
FreezerRegularTrain	97.44	94.35	96.46	96.84	76.07	7.5	86.59
SemgHandSubjectCh2	84.22	85.33	86.14	86.67	20	36.66	89.11
WormsTwoClass	62.34	62.34	61.04	59.74	51.94	46.75	57.14
Earthquakes	74.82	74.82	74.82	74.82	65.46	76.97	76.97
FiftyWords	68.57	68.57	69.67	68.79	34.28	60.21	65.27

A.2 Time Series Regression

For time series regression, we used the 5-fold validation of training set and same hyperparameter sets for all kernels. For training we kernel ridge regression with ridge term chosen from

$$\lambda \in \{0, 0.01, 0.1, 0.2, 0.3, 0.4, 0.5, 0.6, 0.7, 0.8, 0.8, 1, 2, 3, 4, 5, 6, 7, 8, 10, 100\} \quad (47)$$

B Proofs for Theorems 1 and 3: RNTK Convergence at Initialization

B.1 Preliminary: Netsor programs

Calculation of NTK in any architecture relies on finding the GP kernels that correspond to each pre-activation and gradient layers at initialization. For feedforward neural networks with n_1, \dots, n_L number of neurons (channels in CNNs) at each layer the form of this GP kernels can be calculated via taking the limit of n_1, \dots, n_L sequentially one by one. The proof is given by induction, where by conditioning on the previous layers, each entry of the current layer is sum of infinite i.i.d Gaussian random variables, and based on Central Limit Theorem (CLT), it becomes a Gaussian process with kernel calculated based on the previous layers. Since the first layer is an affine transformation of input with Gaussian weights, it is a Gaussian process and the proof is completed. See [15, 17, 26, 31] for a formal treatment. However, due to weight-tiedness (weight sharing), sequential limit is not possible and conditioning on previous layers does not result in i.i.d. weights. Hence the aforementioned arguments break. To deal with it, in [34] a proof using Gaussian conditioning trick [9] is presented which allows use of recurrent weights in a network. More precisely, it has been demonstrated that neural networks (without batch normalization) can be expressed as a series of matrix multiplication and (piece wise) nonlinearity application, generally referred as *Netsor programs*. It has been shown that any architecture that can be expressed as *Netsor programs* that converge to GPs as width goes to infinity in the same rate, which a general rule to obtain the GP kernels. For completeness of this paper, we briefly restate the results from [34] which we will use later for calculation derivation of RNTK.

There are 3 types of variables in *Netsor programs*; *A*-vars, *G*-vars and *H*-vars. *A*-vars are matrices and vectors with i.i.d Gaussian entries, *G*-vars are vectors introduced by multiplication of a vector by an *A*-var and *H*-vars are vectors after coordinate wise nonlinearities is applied to *G*-vars. Generally, *G*-vars can be thought of pre-activation layers which are asymptotically treated as a Gaussian distributed vectors, *H*-vars as after-activation layers and *A*-vars are the weights. Since in neural networks inputs are immediately multiplied by a weight matrix, it can be thought of as an *G*-var, namely \mathbf{g}_{in} . Generally *Netsor programs* supports *G*-vars with different dimension, however the asymptotic behavior of a neural networks described by *Netsor programs* does not change under this degree of freedom, as long as they go to infinity at the same rate. For simplicity, let the *G*-vars and *H*-vars have the same dimension n since the network of interest is RNN and all pre-activation layers have the same dimension. We introduce the *Netsor programs* under this simplification. To produce the output of a neural network, *Netsor programs* receive a set of *G*-vars and *A*-vars as input, and new variables are produced sequentially using the three following operators:

- **Matmul** : multiplication of an *A*-var: \mathbf{A} with an *H*-var: \mathbf{h} , which produce a new *G*-var, \mathbf{g} .

$$\mathbf{g} = \mathbf{A}\mathbf{h} \quad (48)$$

- **Lincomp**: Linear combination of *G*-vars, \mathbf{g}^i , $1 \leq i \leq k$, with coefficients $a^i \in \mathbb{R}$ $1 \leq i \leq k$ which produce of new *G*-var:

$$\mathbf{g} = \sum_{i=1}^k a^i \mathbf{g}^i \quad (49)$$

- **Nonlin**: creating a new *H*-var, \mathbf{h} , by using a nonlinear function $\phi : \mathbb{R}^k \rightarrow \mathbb{R}$ that act coordinate wise on a set of *G*-vars, \mathbf{g}^i , $1 \leq i \leq k$:

$$\mathbf{h} = \varphi(\mathbf{g}^1, \dots, \mathbf{g}^k) \quad (50)$$

Any output of the neural network $y \in \mathbb{R}$ should be expressed as inner product of a new *A*-var which has not been used anywhere else in previous computations and an *H*-var:

$$y = \mathbf{v}^\top \mathbf{h} \quad (51)$$

Any other output can be produced by another \mathbf{v}' and \mathbf{h}' (possibility the same \mathbf{h} or \mathbf{v}).

It is assumed that each entry of any *A*-var : $\mathbf{A} \in \mathbb{R}^{n \times n}$ in the *netsor programs* computations is drawn from $\mathcal{N}(0, \frac{\sigma_a^2}{n})$ and the input *G*-vars are Gaussian distributed. The collection of a specific entry of all *G*-vars of in the

netsor program converges in probability to a Gaussian vector $\{[g^1]_i, \dots, [g^k]_i\} \sim \mathcal{N}(\boldsymbol{\mu}, \boldsymbol{\Sigma})$ for all $i \in [n]$ as n goes to infinity.

Let $\mu(\mathbf{g}) := \mathbb{E}[g]_i$ be the mean of a G -var and $\Sigma(\mathbf{g}, \mathbf{g}') := \mathbb{E}[g]_i \cdot [g']_i$ be the covariance between any two G -vars. The general rule for $\mu(\mathbf{g})$ is given by the following equations:

$$\mu(\mathbf{g}) = \begin{cases} \mu^{\text{in}}(\mathbf{g}) & \text{if } \mathbf{g} \text{ is input} \\ \sum_{i=1}^k a^i \mu(\mathbf{g}^i) & \text{if } \mathbf{g} = \sum_{i=1}^k a^i \mathbf{g}^i \\ 0 & \text{otherwise} \end{cases} \quad (52)$$

For \mathbf{g} and \mathbf{g}' , let $\mathcal{G} = \{\mathbf{g}^1, \dots, \mathbf{g}^r\}$ be the set of G -vars that has been introduced *before* \mathbf{g} and \mathbf{g}' with distribution $\mathcal{N}(\boldsymbol{\mu}_{\mathcal{G}}, \boldsymbol{\Sigma}_{\mathcal{G}})$, where $\boldsymbol{\Sigma}_{\mathcal{G}} \in \mathbb{R}^{|\mathcal{G}| \times |\mathcal{G}|}$ containing the pairwise covariances between the G -vars. $\Sigma(\mathbf{g}, \mathbf{g}')$ is calculated via the following rules:

$$\Sigma(\mathbf{g}, \mathbf{g}') = \begin{cases} \Sigma^{\text{in}}(\mathbf{g}, \mathbf{g}') & \text{if } \mathbf{g} \text{ and } \mathbf{g}' \text{ are inputs} \\ \sum_{i=1}^k a^i \Sigma(\mathbf{g}^i, \mathbf{g}') & \text{if } \mathbf{g} = \sum_{i=1}^k a^i \mathbf{g}^i \\ \sum_{i=1}^k a^i \Sigma(\mathbf{g}, \mathbf{g}^i) & \text{if } \mathbf{g}' = \sum_{i=1}^k a^i \mathbf{g}^i \\ \sigma_A^2 \mathbb{E}_{\mathbf{z} \sim \mathcal{N}(\boldsymbol{\mu}, \boldsymbol{\Sigma}_{\mathcal{G}})} [\varphi(\mathbf{z}) \bar{\varphi}(\mathbf{z})] & \text{if } \mathbf{g} = \mathbf{A}\mathbf{h} \text{ and } \mathbf{g}' = \mathbf{A}\mathbf{h}' \\ 0 & \text{otherwise} \end{cases} \quad (53)$$

Where $\mathbf{h} = \varphi(\mathbf{g}^1, \dots, \mathbf{g}^r)$ and $\mathbf{h}' = \bar{\varphi}(\mathbf{g}^1, \dots, \mathbf{g}^r)$ are functions of G -vars in \mathcal{G} from possibly different nonlinearities. This set of rules presents a recursive method for calculating the GP kernels in a network where the recursive formula starts from data dependent quantities Σ^{in} and μ^{in} which are given.

All the above results holds when the nonlinearities are bounded uniformly by $e^{(cx^2 - \alpha)}$ for some $\alpha > 0$ and when their derivatives exist.

Standard vs. NTK initialization. The common practice (which *netsor programs* uses) is to initialize DNs weights $[\mathbf{A}]_{i,j}$ with $\mathcal{N}(0, \frac{\sigma_a}{\sqrt{n}})$ (known as *standard* initialization) where generally n is the number of units in the previous layer. In this paper we have used a different parameterization scheme as used in [23] and we factor the standard deviation as shown in 7 and initialize weights with standard standard Gaussian. This approach does not change the the forward computation of DN, but normalizes the backward computation (when computing the gradients) by factor $\frac{1}{n}$, otherwise RNTK will be scales by n . However this problem can be solved by scaling the step size by $\frac{1}{n}$ and there is no difference between *NTK* and *standard* initialization [27].

B.2 Proof for Theorem 1: Single layer Case

We first derive the RNTK in a simpler setting, i.e., a single layer and single output RNN. We then generalize the results to multi-layer and multi-output RNNs. We drop the layer index ℓ to simplify notation. From 1 and 7, the forward pass for computing the output under NTK initialization for each input $\mathbf{x} = \{\mathbf{x}_t\}_{t=1}^T$ is given by:

$$\mathbf{g}^{(t)}(\mathbf{x}) = \frac{\sigma_w}{\sqrt{m}} \mathbf{W}\mathbf{h}^{(t-1)}(\mathbf{x}) + \frac{\sigma_u}{\sqrt{n}} \mathbf{U}\mathbf{x}_t + \sigma_b \mathbf{b} \quad (54)$$

$$\mathbf{h}^{(t)}(\mathbf{x}) = \phi\left(\mathbf{g}^{(t)}(\mathbf{x})\right) \quad (55)$$

$$f_{\theta}(\mathbf{x}) = \frac{\sigma_v}{\sqrt{n}} \mathbf{v}^{\top} \mathbf{h}^{(T)}(\mathbf{x}) \quad (56)$$

Note that 54, 55 and 56 use all the introduced operators introduced in 48, 49 and 50 given input variables \mathbf{W} , $\{\mathbf{U}\mathbf{x}_t\}_{t=1}^T$, \mathbf{b} , \mathbf{v} and $\mathbf{h}^{(0)}(\mathbf{x})$.

First, we compute the kernels of forward pass $\Sigma^{(t,t')}(\mathbf{x}, \mathbf{x}')$ and backward pass $\Pi^{(t,t')}(\mathbf{x}, \mathbf{x}')$ introduced in 10 and 11 for two input \mathbf{x} and \mathbf{x}' . Note that based on 52 the mean of all variables is zero since the inputs are all zero mean. In the forward pass for the intermediate layers we have:

$$\Sigma^{(t,t')}(\mathbf{x}, \mathbf{x}') = \Sigma(\mathbf{g}^{(t)}(\mathbf{x}), \mathbf{g}^{(t')}(\mathbf{x}')) \quad (57)$$

$$= \Sigma\left(\frac{\sigma_w}{\sqrt{m}} \mathbf{W}\mathbf{h}^{(t-1)}(\mathbf{x}) + \frac{\sigma_u}{\sqrt{n}} \mathbf{U}\mathbf{x}_t + \sigma_b \mathbf{b}, \frac{\sigma_w}{\sqrt{m}} \mathbf{W}\mathbf{h}^{(t'-1)}(\mathbf{x}') + \frac{\sigma_u}{\sqrt{m}} \mathbf{U}\mathbf{x}'_{t'} + \sigma_b \mathbf{b}\right) \quad (58)$$

$$= \Sigma\left(\frac{\sigma_w}{\sqrt{m}} \mathbf{W}\mathbf{h}^{(t-1)}(\mathbf{x}), \frac{\sigma_w}{\sqrt{m}} \mathbf{W}\mathbf{h}^{(t'-1)}(\mathbf{x}')\right) + \Sigma^{\text{in}}\left(\frac{\sigma_u}{\sqrt{m}} \mathbf{U}\mathbf{x}_t, \frac{\sigma_u}{\sqrt{m}} \mathbf{U}\mathbf{x}'_{t'}\right) + \Sigma^{\text{in}}(\sigma_b \mathbf{b}, \sigma_b \mathbf{b}). \quad (59)$$

We have used the second and third rule in 53 to expand the formula, We have also used the first and fifth rule to set the cross term to zero, i.e.,

$$\Sigma \left(\frac{\sigma_w}{\sqrt{n}} \mathbf{W} \mathbf{h}^{(t-1)}(\mathbf{x}), \frac{\sigma_u}{\sqrt{n}} \mathbf{U} \mathbf{x}'_{t'} \right) = 0 \quad (60)$$

$$\Sigma \left(\frac{\sigma_w}{\sqrt{n}} \mathbf{W} \mathbf{h}^{(t-1)}(\mathbf{x}), \sigma_b \mathbf{b} \right) = 0 \quad (61)$$

$$\Sigma \left(\frac{\sigma_u}{\sqrt{m}} \mathbf{U} \mathbf{x}_t, \frac{\sigma_w}{\sqrt{n}} \mathbf{W} \mathbf{h}^{(t'-1)}(\mathbf{x}') \right) = 0 \quad (62)$$

$$\Sigma \left(\sigma_b \mathbf{b}, \frac{\sigma_w}{\sqrt{n}} \mathbf{W} \mathbf{h}^{(t'-1)}(\mathbf{x}') \right) = 0 \quad (63)$$

$$\Sigma^{\text{in}} \left(\frac{\sigma_u}{\sqrt{m}} \mathbf{U} \mathbf{x}_t, \sigma_b \mathbf{b} \right) = 0 \quad (64)$$

$$\Sigma^{\text{in}} \left(\sigma_b \mathbf{b}, \frac{\sigma_u}{\sqrt{m}} \mathbf{U} \mathbf{x}'_{t'} \right) = 0. \quad (65)$$

For the non-zero terms we have

$$\Sigma^{\text{in}}(\sigma_b \mathbf{b}, \sigma_b \mathbf{b}) = \sigma_b^2 \quad (66)$$

$$\Sigma^{\text{in}} \left(\frac{\sigma_u}{\sqrt{m}} \mathbf{U} \mathbf{x}_t, \frac{\sigma_u}{\sqrt{m}} \mathbf{U} \mathbf{x}'_{t'} \right) = \frac{\sigma_u^2}{m} \langle \mathbf{x}_t, \mathbf{x}'_{t'} \rangle, \quad (67)$$

which can be achieved by straight forward computation. And by using the fourth rule in 53 we have

$$\Sigma \left(\frac{\sigma_w}{\sqrt{n}} \mathbf{W} \mathbf{h}^{(t-1)}(\mathbf{x}), \frac{\sigma_w}{\sqrt{n}} \mathbf{W} \mathbf{h}^{(t'-1)}(\mathbf{x}') \right) = \sigma_w^2 \mathbb{E}_{\mathbf{z} \sim \mathcal{N}(0, \mathbf{K}^{(t,t')}(\mathbf{x}, \mathbf{x}'))} [\phi(z_1) \phi(z_2)] = \text{V}_\phi[\mathbf{K}^{(t,t')}(\mathbf{x}, \mathbf{x}')]. \quad (68)$$

With $\mathbf{K}^{(t,t')}(\mathbf{x}, \mathbf{x}')$ defined in 18. Here the set of previously introduced G -vars is $\mathcal{G} = \{\{\mathbf{g}^{(\alpha)}(\mathbf{x})\}, \mathbf{U} \mathbf{x}_\alpha\}_{\alpha=1}^{t-1}, \{\mathbf{g}^{(\alpha')}(\mathbf{x}'), \mathbf{U} \mathbf{x}'_{\alpha'}\}_{\alpha'=1}^{t'-1}, \mathbf{h}^{(0)}(\mathbf{x}), \mathbf{h}^{(0)}(\mathbf{x}')\}$, but the dependency is only on the last layer G -vars, $\varphi(\{\mathbf{g} : \mathbf{g} \in \mathcal{G}\}) = \phi(\mathbf{g}^{(t-1)}(\mathbf{x}))$, $\bar{\varphi}(\{\mathbf{g} : \mathbf{g} \in \mathcal{G}\}) = \phi(\mathbf{g}^{(t'-1)}(\mathbf{x}'))$, leading the calculation to the operator defined in 14. As a result

$$\Sigma^{(t,t')}(\mathbf{x}, \mathbf{x}') = \sigma_w^2 \text{V}_\phi[\mathbf{K}^{(t,t')}(\mathbf{x}, \mathbf{x}')] + \frac{\sigma_u^2}{m} \langle \mathbf{x}_t, \mathbf{x}'_{t'} \rangle + \sigma_b^2. \quad (69)$$

To complete the recursive formula, using the same procedure for the first layer we have

$$\Sigma^{(1,1)}(\mathbf{x}, \mathbf{x}') = \sigma_w^2 \sigma_h^2 1_{(\mathbf{x}=\mathbf{x}')} + \frac{\sigma_u^2}{m} \langle \mathbf{x}_1, \mathbf{x}'_1 \rangle + \sigma_b^2. \quad (70)$$

The output GP kernel is calculated via

$$\mathcal{K}(\mathbf{x}, \mathbf{x}') = \sigma_v^2 \text{V}_\phi[\mathbf{K}^{(T+1,T'+1)}(\mathbf{x}, \mathbf{x}')] \quad (71)$$

The calculation of the gradient vectors $\boldsymbol{\delta}^{(t)}(\mathbf{x}) = \sqrt{n}(\nabla_{\mathbf{g}^{(t)}(\mathbf{x})} f_\theta(\mathbf{x}))$ in the backward pass is given by

$$\boldsymbol{\delta}^{(T)}(\mathbf{x}) = \sigma_v \mathbf{v} \odot \phi'(\mathbf{g}^{(T)}(\mathbf{x})) \quad (72)$$

$$\boldsymbol{\delta}^{(t)}(\mathbf{x}) = \frac{\sigma_w}{\sqrt{n}} \mathbf{W}^\top \left(\phi'(\mathbf{g}^{(t)}(\mathbf{x})) \odot \boldsymbol{\delta}^{(t+1)}(\mathbf{x}) \right) \quad t \in [T-1] \quad (73)$$

To calculate the backward pass kernels, we rely on the following Corollary.

Corollary 1 ([34]) *In infinitely wide neural networks weights used in calculation of back propagation gradients (\mathbf{W}^\top) is an i.i.d copy of weights used in forward propagation (\mathbf{W}) as long as the last layer weight (\mathbf{v}) is sampled independently from other parameters and has mean 0.*

The immediate result of Corollary 1 is that $\mathbf{g}^{(t)}(\mathbf{x})$ and $\boldsymbol{\delta}^{(t)}(\mathbf{x})$ are two independent Gaussian vector as their covariance is zero based on the fifth rule in 53. Using this result, we have:

$$\Pi^{(t,t')}(\mathbf{x}, \mathbf{x}') = \Sigma \left(\boldsymbol{\delta}^{(t)}(\mathbf{x}), \boldsymbol{\delta}^{(t')}(\mathbf{x}') \right) \quad (74)$$

$$= \mathbb{E} \left[[\boldsymbol{\delta}^{(t)}(\mathbf{x})]_i \cdot [\boldsymbol{\delta}^{(t')}(\mathbf{x}')]_i \right] \quad (75)$$

$$= \sigma_w^2 \mathbb{E} \left[[\phi'(\mathbf{g}^{(t)}(\mathbf{x}))]_i \cdot [\boldsymbol{\delta}^{(t+1)}(\mathbf{x})]_i \cdot [\phi'(\mathbf{g}^{(t')}(\mathbf{x}'))]_i \cdot [\boldsymbol{\delta}^{(t'+1)}(\mathbf{x}')]_i \right] \quad (76)$$

$$= \sigma_w^2 \mathbb{E}_{\mathbf{z} \sim \mathcal{N}(0, \mathbf{K}^{(t+1,t'+1)}(\mathbf{x}, \mathbf{x}'))} [\phi'(z_1) \cdot \phi'(z_2)] \cdot \mathbb{E} \left[[\boldsymbol{\delta}^{(t+1)}(\mathbf{x})]_i \cdot [\boldsymbol{\delta}^{(t'+1)}(\mathbf{x}')]_i \right] \quad (77)$$

$$= \sigma_w^2 \text{V}_{\phi'}[\mathbf{K}^{(t+1,t'+1)}(\mathbf{x}, \mathbf{x}')] \Pi^{(t+1,t'+1)}(\mathbf{x}, \mathbf{x}'). \quad (78)$$

If $T' - t' = T - t$, then the formula will lead to

$$\Pi^{(T, T')}(\mathbf{x}, \mathbf{x}') = \mathbb{E} \left[[\boldsymbol{\delta}^{(T)}(\mathbf{x})]_i, [\boldsymbol{\delta}^{(T')}(\mathbf{x}')]_i \right] \quad (79)$$

$$= \sigma_v^2 \mathbb{E} \left[[\mathbf{v}]_i \cdot [\phi'(\mathbf{g}^{(T)}(\mathbf{x}))]_i \cdot [\mathbf{v}]_i \cdot [\phi'(\mathbf{g}^{(T')}(\mathbf{x}'))]_i \right] \quad (80)$$

$$= \mathbb{E} \left[[\phi'(\mathbf{g}^{(T)}(\mathbf{x}))]_i \cdot [\phi'(\mathbf{g}^{(T')}(\mathbf{x}'))]_i \right] \cdot \mathbb{E} \left[[\mathbf{v}]_i [\mathbf{v}]_i \right] \quad (81)$$

$$= \sigma_v^2 \mathbf{V}_{\phi'} [\mathbf{K}^{(T+1, T+\tau+1)}(\mathbf{x}, \mathbf{x}')]. \quad (82)$$

Otherwise it will end to either of two cases for some $t'' < T$ or T' and by the fifth rule in 53 we have:

$$\Sigma \left(\boldsymbol{\delta}^{(t'')}(\mathbf{x}), \boldsymbol{\delta}^{(T')}(\mathbf{x}') \right) = \Sigma \left(\frac{\sigma_w}{\sqrt{n}} \mathbf{W}^\top \left(\phi'(\mathbf{g}^{(t'')}(\mathbf{x})) \odot \boldsymbol{\delta}^{(t''+1)}(\mathbf{x}') \right), \mathbf{v} \odot \phi'(\mathbf{g}^{(T')}(\mathbf{x}')) \right) = 0 \quad (83)$$

$$\Sigma \left(\boldsymbol{\delta}^{(T)}(\mathbf{x}), \boldsymbol{\delta}^{(t'')}(\mathbf{x}') \right) = \Sigma \left(\mathbf{v} \odot \phi'(\mathbf{g}^{(T)}(\mathbf{x})), \frac{\sigma_w}{\sqrt{n}} \mathbf{W}^\top \left(\phi'(\mathbf{g}^{(t'')}(\mathbf{x}')) \odot \boldsymbol{\delta}^{(t''+1)}(\mathbf{x}') \right) \right) = 0. \quad (84)$$

Without loss of generality, from now on assume $T' < T$ and $T' - T = \tau$, the final formula for computing the backward gradients becomes:

$$\Pi^{(T, T+\tau)}(\mathbf{x}, \mathbf{x}') = \sigma_v^2 \mathbf{V}_{\phi'} [\mathbf{K}^{(T+1, T+\tau+1)}(\mathbf{x}, \mathbf{x}')] \quad (85)$$

$$\Pi^{(t, t+\tau)}(\mathbf{x}, \mathbf{x}') = \sigma_w^2 \mathbf{V}_{\phi'} [\mathbf{K}^{(t+1, t+\tau+1)}(\mathbf{x}, \mathbf{x}')] \Pi^{(t+1, t+1+\tau)}(\mathbf{x}, \mathbf{x}') \quad t \in [T-1] \quad (86)$$

$$\Pi^{(t, t')}(\mathbf{x}, \mathbf{x}') = 0 \quad t' - t \neq \tau \quad (87)$$

Now we have derived the single layer RNTK. Recall that $\theta = \text{Vect}[\{\mathbf{W}, \mathbf{U}, \mathbf{b}, \mathbf{v}\}]$ contains all of the network's learnable parameters. As a result, we have:

$$\nabla_{\theta} f_{\theta}(\mathbf{x}) = \text{Vect} \left[\left\{ \frac{\partial f_{\theta}(\mathbf{x})}{\partial \mathbf{W}}, \frac{\partial f_{\theta}(\mathbf{x})}{\partial \mathbf{U}}, \frac{\partial f_{\theta}(\mathbf{x})}{\partial \mathbf{b}}, \frac{\partial f_{\theta}(\mathbf{x})}{\partial \mathbf{v}} \right\} \right]. \quad (88)$$

As a result

$$\langle \nabla_{\theta} f_{\theta}(\mathbf{x}), \nabla_{\theta} f_{\theta}(\mathbf{x}') \rangle = \left\langle \frac{\partial f_{\theta}(\mathbf{x})}{\partial \mathbf{W}}, \frac{\partial f_{\theta}(\mathbf{x}')}{\partial \mathbf{W}} \right\rangle + \left\langle \frac{\partial f_{\theta}(\mathbf{x})}{\partial \mathbf{U}}, \frac{\partial f_{\theta}(\mathbf{x}')}{\partial \mathbf{U}} \right\rangle + \left\langle \frac{\partial f_{\theta}(\mathbf{x})}{\partial \mathbf{b}}, \frac{\partial f_{\theta}(\mathbf{x}')}{\partial \mathbf{b}} \right\rangle \quad (89)$$

$$+ \left\langle \frac{\partial f_{\theta}(\mathbf{x})}{\partial \mathbf{v}}, \frac{\partial f_{\theta}(\mathbf{x}')}{\partial \mathbf{v}} \right\rangle \quad (90)$$

Where the gradients of output with respect to weights can be formulated as the following compact form:

$$\frac{\partial f_{\theta}(\mathbf{x})}{\partial \mathbf{W}} = \sum_{t=1}^T \left(\frac{1}{\sqrt{n}} \boldsymbol{\delta}^{(t)}(\mathbf{x}) \right) \cdot \left(\frac{\sigma_w}{\sqrt{n}} \mathbf{h}^{(t-1)}(\mathbf{x}) \right)^\top \quad (91)$$

$$\frac{\partial f_{\theta}(\mathbf{x})}{\partial \mathbf{U}} = \sum_{t=1}^T \left(\frac{1}{\sqrt{n}} \boldsymbol{\delta}^{(t)}(\mathbf{x}) \right) \cdot \left(\frac{\sigma_u}{\sqrt{m}} \mathbf{x}_t \right)^\top \quad (92)$$

$$\frac{\partial f_{\theta}(\mathbf{x})}{\partial \mathbf{b}} = \sum_{t=1}^T \left(\frac{\sigma_b}{\sqrt{n}} \boldsymbol{\delta}^{(t)}(\mathbf{x}) \right) \quad (93)$$

$$\frac{\partial f_{\theta}(\mathbf{x})}{\partial \mathbf{v}} = \frac{\sigma_v}{\sqrt{n}} \mathbf{h}^{(T)}(\mathbf{x}). \quad (94)$$

As a result we have:

$$\left\langle \frac{\partial f_{\theta}(\mathbf{x})}{\partial \mathbf{W}}, \frac{\partial f_{\theta}(\mathbf{x}')}{\partial \mathbf{W}} \right\rangle = \sum_{t'=1}^{T'} \sum_{t=1}^T \left(\frac{1}{n} \langle \boldsymbol{\delta}^{(t)}(\mathbf{x}), \boldsymbol{\delta}^{(t')}(\mathbf{x}') \rangle \right) \cdot \left(\frac{\sigma_w^2}{n} \langle \mathbf{h}^{(t-1)}(\mathbf{x}), \mathbf{h}^{(t'-1)}(\mathbf{x}') \rangle \right) \quad (95)$$

$$\left\langle \frac{\partial f_{\theta}(\mathbf{x})}{\partial \mathbf{U}}, \frac{\partial f_{\theta}(\mathbf{x}')}{\partial \mathbf{U}} \right\rangle = \sum_{t'=1}^{T'} \sum_{t=1}^T \left(\frac{1}{n} \langle \boldsymbol{\delta}^{(t)}(\mathbf{x}), \boldsymbol{\delta}^{(t')}(\mathbf{x}') \rangle \right) \cdot \left(\frac{\sigma_u^2}{m} \langle \mathbf{x}_t, \mathbf{x}'_{t'} \rangle \right) \quad (96)$$

$$\left\langle \frac{\partial f_{\theta}(\mathbf{x})}{\partial \mathbf{b}}, \frac{\partial f_{\theta}(\mathbf{x}')}{\partial \mathbf{b}} \right\rangle = \sum_{t'=1}^{T'} \sum_{t=1}^T \left(\frac{1}{n} \langle \boldsymbol{\delta}^{(t)}(\mathbf{x}), \boldsymbol{\delta}^{(t')}(\mathbf{x}') \rangle \right) \cdot \sigma_b^2 \quad (97)$$

$$\left\langle \frac{\partial f_{\theta}(\mathbf{x})}{\partial \mathbf{v}}, \frac{\partial f_{\theta}(\mathbf{x}')}{\partial \mathbf{v}} \right\rangle = \left(\frac{\sigma_v^2}{n} \langle \mathbf{h}^{(T)}(\mathbf{x}), \mathbf{h}^{(T')}(\mathbf{x}') \rangle \right). \quad (98)$$

Remember that for any two G -var $\mathbb{E}[[\mathbf{g}]_i[\mathbf{g}']_i]$ is independent of index i . Therefore,

$$\frac{1}{n} \langle \mathbf{h}^{(t-1)}(\mathbf{x}), \mathbf{h}^{(t-1)}(\mathbf{x}') \rangle \rightarrow \text{V}_\phi[\mathbf{K}^{(t,t')}(\mathbf{x}, \mathbf{x}')] \quad t > 1 \quad (99)$$

$$\frac{1}{n} \langle \mathbf{h}^{(0)}(\mathbf{x}), \mathbf{h}^{(0)}(\mathbf{x}') \rangle \rightarrow \sigma_h^2. \quad (100)$$

Hence, by summing the above terms in the infinite width limit we get

$$\langle \nabla_\theta f_\theta(\mathbf{x}), \nabla_\theta f_\theta(\mathbf{x}') \rangle \rightarrow \left(\sum_{t'=1}^{T'} \sum_{t=1}^T \Pi^{(t,t')}(\mathbf{x}, \mathbf{x}') \cdot \Sigma^{(t,t')}(\mathbf{x}', \mathbf{x}') \right) + \mathcal{K}(\mathbf{x}, \mathbf{x}'). \quad (101)$$

Since $\Pi^{(t,t')}(\mathbf{x}, \mathbf{x}') = 0$ for $t' - t \neq \tau$ it is simplified to

$$\langle \nabla_\theta f_\theta(\mathbf{x}), \nabla_\theta f_\theta(\mathbf{x}') \rangle = \left(\sum_{t=1}^T \Pi^{(t,t+\tau)}(\mathbf{x}, \mathbf{x}') \cdot \Sigma^{(t,t+\tau)}(\mathbf{x}', \mathbf{x}') \right) + \mathcal{K}(\mathbf{x}, \mathbf{x}'). \quad (102)$$

Multi-dimensional output. For $f_\theta(\mathbf{x}) \in \mathbb{R}^d$, the i -th output for $i \in [d]$ is obtained via

$$[f_\theta(\mathbf{x})]_i = \frac{\sigma_v}{\sqrt{n}} \mathbf{v}_i^\top \mathbf{h}^{(T)}(\mathbf{x}), \quad (103)$$

where \mathbf{v}_i is independent of \mathbf{v}_j for $i \neq j$. As a result, for The RNTK $\Theta(\mathbf{x}, \mathbf{x}') \in \mathbb{R}^{d \times d}$ for multi-dimensional output we have

$$[\Theta(\mathbf{x}, \mathbf{x}')]_{i,j} = \langle \nabla_\theta [f_\theta(\mathbf{x})]_i, \nabla_\theta [f_\theta(\mathbf{x}')]_j \rangle \quad (104)$$

For $i = j$, the kernel is the same as computed in 101 and we denote it as

$$\langle \nabla_\theta [f_\theta(\mathbf{x})]_i, \nabla_\theta [f_\theta(\mathbf{x}')]_i \rangle = \Theta^{(T,T')}(\mathbf{x}, \mathbf{x}'). \quad (105)$$

For $i \neq j$, since \mathbf{v}_i is independent of \mathbf{v}_j , $\Pi^{(T,T')}(\mathbf{x}, \mathbf{x}')$ and all the backward pass gradients become zero, so

$$\langle \nabla_\theta [f_\theta(\mathbf{x})]_i, \nabla_\theta [f_\theta(\mathbf{x}')]_j \rangle = 0 \quad i \neq j \quad (106)$$

which gives us the following formula

$$\Theta(\mathbf{x}, \mathbf{x}') = \Theta^{(T,T')}(\mathbf{x}, \mathbf{x}') \otimes \mathbf{I}_d. \quad (107)$$

This concludes the proof for Theorem 1 for single-layer case.

B.3 Proof for Theorem 1: Multi-Layer Case

Now we drive the RNTK for multi-layer RNTK. We will only study single output case and the generalization to multi-dimensional case is identical as the single layer case. The set of equations for calculation of the output of a L -layer RNN for $\mathbf{x} = \{\mathbf{x}_t\}_{t=1}^T$ are

$$\mathbf{g}^{(\ell,t)}(\mathbf{x}) = \frac{\sigma_w^\ell}{\sqrt{n}} \mathbf{W}^{(\ell)} \mathbf{h}^{(\ell,t-1)}(\mathbf{x}) + \frac{\sigma_u^\ell}{\sqrt{m}} \mathbf{U}^{(\ell)} \mathbf{x}_t + \sigma_b^\ell \mathbf{b}^{(\ell)} \quad \ell = 1 \quad (108)$$

$$\mathbf{g}^{(\ell,t)}(\mathbf{x}) = \frac{\sigma_w^\ell}{\sqrt{n}} \mathbf{W}^{(\ell)} \mathbf{h}^{(\ell,t-1)}(\mathbf{x}) + \frac{\sigma_u^\ell}{\sqrt{n}} \mathbf{U}^{(\ell)} \mathbf{h}^{(\ell-1,t)}(\mathbf{x}) + \sigma_b^\ell \mathbf{b}^{(\ell)} \quad \ell > 1 \quad (109)$$

$$\mathbf{h}^{(\ell,t)}(\mathbf{x}) = \phi(\mathbf{g}^{(\ell,t)}(\mathbf{x})) \quad (110)$$

$$f_\theta(\mathbf{x}) = \frac{\sigma_v}{\sqrt{n}} \mathbf{v}^\top \mathbf{h}^{(L,T)}(\mathbf{x}) \quad (111)$$

The forward pass kernels for the first layer is the same as calculated in B.2. For $\ell \geq 2$ we have:

$$\Sigma^{(\ell,t,t')}(\mathbf{x}, \mathbf{x}') = \Sigma(\mathbf{g}^{(\ell,t)}(\mathbf{x}), \mathbf{g}^{(\ell,t')}(\mathbf{x}')) \quad (112)$$

$$= \Sigma \left(\frac{\sigma_w^\ell}{\sqrt{n}} \mathbf{W}^{(\ell)} \mathbf{h}^{(\ell,t-1)}(\mathbf{x}), \frac{\sigma_w^\ell}{\sqrt{n}} \mathbf{W}^{(\ell)} \mathbf{h}^{(\ell,t'-1)}(\mathbf{x}') \right) \quad (113)$$

$$+ \Sigma \left(\frac{\sigma_u^\ell}{\sqrt{n}} \mathbf{U}^{(\ell)} \mathbf{h}^{(\ell-1,t)}(\mathbf{x}), \frac{\sigma_u^\ell}{\sqrt{n}} \mathbf{U}^{(\ell)} \mathbf{h}^{(\ell-1,t')}(\mathbf{x}') \right) + \Sigma^{\text{in}}(\sigma_b^\ell \mathbf{b}^{(\ell)}, \sigma_b^\ell \mathbf{b}^{(\ell)}) \quad (114)$$

$$= (\sigma_w^\ell)^2 \text{V}_\phi[\mathbf{K}^{(\ell,t,t')}(\mathbf{x}, \mathbf{x}')] + (\sigma_u^\ell)^2 \text{V}_\phi[\mathbf{K}^{(\ell-1,t+1,t'+1)}(\mathbf{x}, \mathbf{x}')] + (\sigma_b^\ell)^2, \quad (115)$$

where

$$\mathbf{K}^{(\ell,t,t')}(\mathbf{x}, \mathbf{x}') = \begin{bmatrix} \Sigma^{(\ell,t-1,t-1)}(\mathbf{x}, \mathbf{x}) & \Sigma^{(\ell,t-1,t'-1)}(\mathbf{x}, \mathbf{x}') \\ \Sigma^{(\ell,t-1,t'-1)}(\mathbf{x}, \mathbf{x}') & \Sigma^{(\ell,t'-1,t'-1)}(\mathbf{x}', \mathbf{x}') \end{bmatrix}, \quad (116)$$

and Σ^{in} is defined in 66. For the first first time step we have:

$$\Sigma^{(\ell,1,1)}(\mathbf{x}, \mathbf{x}') = (\sigma_w^\ell)^2 \sigma_h^2 \mathbf{1}_{(\mathbf{x}=\mathbf{x}')} + (\sigma_u^\ell)^2 \text{V}_\phi[\mathbf{K}^{(\ell,2,2)}(\mathbf{x}, \mathbf{x}')] + (\sigma_b^\ell)^2, \quad (117)$$

and the output layer

$$\mathcal{K}(\mathbf{x}, \mathbf{x}') = \sigma_v^2 \text{V}_\phi[\mathbf{K}^{(L,T+1,T'+1)}(\mathbf{x}, \mathbf{x}')]. \quad (118)$$

Note that because of using new weights at each layer we get

$$\Sigma(\mathbf{g}^{(\ell,t)}(\mathbf{x}), \mathbf{g}^{(\ell',t')}(\mathbf{x})) = 0 \quad \ell \neq \ell' \quad (119)$$

Now we calculate the backward pass kernels in multi-layer RNTK. The gradients at the last layer is calculated via

$$\delta^{(L,T)}(\mathbf{x}) = \sigma_v \mathbf{v} \odot \phi'(\mathbf{g}^{(L,T)}(\mathbf{x})). \quad (120)$$

In the last hidden layer for different time steps we have

$$\delta^{(L,t)}(\mathbf{x}) = \frac{\sigma_w^L}{\sqrt{n}} \left(\mathbf{W}^{(L)} \right)^\top \left(\phi'(\mathbf{g}^{(L,t)}(\mathbf{x})) \odot \delta^{(L,t+1)}(\mathbf{x}) \right) \quad t \in [T-1] \quad (121)$$

In the last time step for different hidden layers we have

$$\delta^{(\ell,T)}(\mathbf{x}) = \frac{\sigma_u^{\ell+1}}{\sqrt{n}} \left(\mathbf{U}^{(\ell+1)} \right)^\top \left(\phi'(\mathbf{g}^{(\ell,T)}(\mathbf{x})) \odot \delta^{(\ell+1,T)}(\mathbf{x}) \right) \quad \ell \in [L-1] \quad (122)$$

At the end for the other layers we have

$$\delta^{(\ell,t)}(\mathbf{x}) = \frac{\sigma_w^\ell}{\sqrt{n}} \left(\mathbf{W}^{(\ell)} \right)^\top \left(\phi'(\mathbf{g}^{(\ell,t)}(\mathbf{x})) \odot \delta^{(\ell,t+1)}(\mathbf{x}) \right) \quad (123)$$

$$+ \frac{\sigma_u^{\ell+1}}{\sqrt{n}} \left(\mathbf{U}^{(\ell+1)} \right)^\top \left(\phi'(\mathbf{g}^{(\ell,t)}(\mathbf{x})) \odot \delta^{(\ell+1,t)}(\mathbf{x}) \right) \quad \ell \in [L-1], t \in [T-1] \quad (124)$$

The recursive formula for the $\Pi^{(L,t,t')}(\mathbf{x}, \mathbf{x}')$ is the same as the single layer, and it is non-zero for $t' - t = T' - T = \tau$. As a result we have

$$\Pi^{(L,T,T+\tau)}(\mathbf{x}, \mathbf{x}') = \sigma_v^2 \text{V}_{\phi'}[\mathbf{K}^{(L,T+1,T+\tau+1)}](\mathbf{x}, \mathbf{x}') \quad (125)$$

$$\Pi^{(L,t,t+\tau)}(\mathbf{x}, \mathbf{x}') = (\sigma_w^L)^2 \text{V}_{\phi'}[\mathbf{K}^{(L,t+1,t+\tau+1)}](\mathbf{x}, \mathbf{x}') \cdot \Pi^{(L,t+1,t+1+\tau)}(\mathbf{x}, \mathbf{x}') \quad t \in [T-1] \quad (126)$$

$$\Pi^{(L,t,t')}(\mathbf{x}, \mathbf{x}') = 0 \quad t' - t \neq \tau \quad (127)$$

Similarly by using the same course of arguments used in the single layer setting, for the last time step we have

$$\Pi^{(\ell,T,T+\tau)}(\mathbf{x}, \mathbf{x}') = (\sigma_u^{\ell+1})^2 \text{V}_{\phi'}[\mathbf{K}^{(\ell,T+1,T+\tau+1)}](\mathbf{x}, \mathbf{x}') \cdot \Pi^{(\ell+1,T+1,T+\tau+1)}(\mathbf{x}, \mathbf{x}') \quad \ell \in [L-1] \quad (128)$$

For the other layers we have

$$\Pi^{(\ell,t,t')}(\mathbf{x}, \mathbf{x}') = (\sigma_w^\ell)^2 \text{V}_{\phi'}[\mathbf{K}^{(\ell,t+1,t+\tau+1)}](\mathbf{x}, \mathbf{x}') \cdot \Pi^{(\ell,t+1,t+1+\tau)}(\mathbf{x}, \mathbf{x}') \quad (129)$$

$$+ (\sigma_u^{\ell+1})^2 \text{V}_{\phi'}[\mathbf{K}^{(\ell,t+1,t+\tau+1)}](\mathbf{x}, \mathbf{x}') \cdot \Pi^{(\ell+1,t+1,t'+1)}(\mathbf{x}, \mathbf{x}'). \quad (130)$$

For $t' - t \neq \tau$ the recursion continues until it reaches $\Pi^{(L,T,t'')(\mathbf{x}, \mathbf{x}')$, $t'' < T'$ or $\Pi^{(L,t'',T')(\mathbf{x}, \mathbf{x}')$, $t'' < T$ and as a result based on 127 we get

$$\Pi^{(\ell,t,t')}(\mathbf{x}, \mathbf{x}') = 0 \quad t' - t \neq \tau \quad (131)$$

For $t' - t = \tau$ it leads to $\Pi^{(L,T,T')(\mathbf{x}, \mathbf{x}')$ and has a non-zero value.

Now we derive RNTK for multi-layer:

$$\langle \nabla_{\theta} f_{\theta}(\mathbf{x}), \nabla_{\theta} f_{\theta}(\mathbf{x}') \rangle = \sum_{\ell=1}^L \left\langle \frac{\partial f_{\theta}(\mathbf{x})}{\partial \mathbf{W}^{(\ell)}}, \frac{\partial f_{\theta}(\mathbf{x}')}{\partial \mathbf{W}^{(\ell)}} \right\rangle + \sum_{\ell=1}^L \left\langle \frac{\partial f_{\theta}(\mathbf{x})}{\partial \mathbf{U}^{(\ell)}}, \frac{\partial f_{\theta}(\mathbf{x}')}{\partial \mathbf{U}^{(\ell)}} \right\rangle \quad (132)$$

$$+ \sum_{\ell=1}^L \left\langle \frac{\partial f_{\theta}(\mathbf{x})}{\partial \mathbf{b}^{(\ell)}}, \frac{\partial f_{\theta}(\mathbf{x}')}{\partial \mathbf{b}^{(\ell)}} \right\rangle + \left\langle \frac{\partial f_{\theta}(\mathbf{x})}{\partial \mathbf{v}}, \frac{\partial f_{\theta}(\mathbf{x}')}{\partial \mathbf{v}} \right\rangle, \quad (133)$$

where

$$\left\langle \frac{\partial f_\theta(\mathbf{x})}{\partial \mathbf{W}^{(\ell)}}, \frac{\partial f_\theta(\mathbf{x}')}{\partial \mathbf{W}^{(\ell)}} \right\rangle = \sum_{t'=1}^{T'} \sum_{t=1}^T \left(\frac{1}{n} \langle \boldsymbol{\delta}^{(\ell,t)}(\mathbf{x}), \boldsymbol{\delta}^{(\ell,t')}(\mathbf{x}') \rangle \right) \cdot \left(\frac{(\sigma_w^\ell)^2}{n} \langle \mathbf{h}^{(\ell,t-1)}(\mathbf{x}), \mathbf{h}^{(\ell,t'-1)}(\mathbf{x}') \rangle \right) \quad (134)$$

$$\left\langle \frac{\partial f_\theta(\mathbf{x})}{\partial \mathbf{U}^{(\ell)}}, \frac{\partial f_\theta(\mathbf{x}')}{\partial \mathbf{U}^{(\ell)}} \right\rangle = \sum_{t'=1}^{T'} \sum_{t=1}^T \left(\frac{1}{n} \langle \boldsymbol{\delta}^{(\ell,t)}(\mathbf{x}), \boldsymbol{\delta}^{(\ell,t')}(\mathbf{x}') \rangle \right) \cdot \left(\frac{(\sigma_u^\ell)^2}{m} \langle \mathbf{x}_t, \mathbf{x}'_{t'} \rangle \right) \quad \ell = 1 \quad (135)$$

$$\left\langle \frac{\partial f_\theta(\mathbf{x})}{\partial \mathbf{U}^{(\ell)}}, \frac{\partial f_\theta(\mathbf{x}')}{\partial \mathbf{U}^{(\ell)}} \right\rangle = \sum_{t'=1}^{T'} \sum_{t=1}^T \left[\left(\frac{1}{n} \langle \boldsymbol{\delta}^{(\ell,t)}(\mathbf{x}), \boldsymbol{\delta}^{(\ell,t')}(\mathbf{x}') \rangle \right) \right. \quad (136)$$

$$\left. \cdot \left(\frac{(\sigma_u^\ell)^2}{n} \langle \mathbf{h}^{(\ell-1,t)}(\mathbf{x}), \mathbf{h}^{(\ell-1,t')}(\mathbf{x}') \rangle \right) \right] \quad \ell > 1 \quad (137)$$

$$\left\langle \frac{\partial f_\theta(\mathbf{x})}{\partial \mathbf{b}^{(\ell)}}, \frac{\partial f_\theta(\mathbf{x}')}{\partial \mathbf{b}^{(\ell)}} \right\rangle = \sum_{t'=1}^{T'} \sum_{t=1}^T \left(\frac{1}{n} \langle \boldsymbol{\delta}^{(\ell,t)}(\mathbf{x}), \boldsymbol{\delta}^{(\ell,t')}(\mathbf{x}') \rangle \right) \cdot (\sigma_b^\ell)^2 \quad (138)$$

$$\left\langle \frac{\partial f_\theta(\mathbf{x})}{\partial \mathbf{v}}, \frac{\partial f_\theta(\mathbf{x}')}{\partial \mathbf{v}} \right\rangle = \left(\frac{\sigma_v^2}{n} \langle \mathbf{h}^{(T)}(\mathbf{x}), \mathbf{h}^{(T')}(\mathbf{x}') \rangle \right) \quad (139)$$

Summing up all the terms and replacing the inner product of vectors with their expectations we get

$$\langle \nabla_\theta f_\theta(\mathbf{x}), \nabla_\theta f_\theta(\mathbf{x}') \rangle = \Theta^{(L,T,T')} = \left(\sum_{\ell=1}^L \sum_{t=1}^T \sum_{t'=1}^{T'} \Pi^{(\ell,t,t')}(\mathbf{x}, \mathbf{x}') \cdot \Sigma^{(\ell,t,t')}(\mathbf{x}, \mathbf{x}') \right) + \mathcal{K}(\mathbf{x}, \mathbf{x}'). \quad (140)$$

By (131), we can simplify to

$$\Theta^{(L,T,T')} = \left(\sum_{\ell=1}^L \sum_{t=1}^T \Pi^{(\ell,t,t')}(\mathbf{x}, \mathbf{x}') \cdot \Sigma^{(\ell,t,t+\tau)}(\mathbf{x}, \mathbf{x}') \right) + \mathcal{K}(\mathbf{x}, \mathbf{x}'). \quad (141)$$

For multi-dimensional output it becomes

$$\Theta(\mathbf{x}, \mathbf{x}') = \Theta^{(L,T,T')}(\mathbf{x}, \mathbf{x}') \otimes \mathbf{I}_d. \quad (142)$$

This concludes the proof for Theorem 1 for the multi-layer case.

B.4 Proof for Theorem 3: Weight-Untied RNTK

The architecture of a weight-untied single layer RNN is

$$\mathbf{g}^{(t)}(\mathbf{x}) = \frac{\sigma_w}{\sqrt{m}} \mathbf{W}^{(t)} \mathbf{h}^{(t-1)}(\mathbf{x}) + \frac{\sigma_u}{\sqrt{n}} \mathbf{U}^{(t)} \mathbf{x}_t + \sigma_b \mathbf{b}^{(t)} \quad (143)$$

$$\mathbf{h}^{(t)}(\mathbf{x}) = \phi(\mathbf{g}^{(t)}(\mathbf{x})) \quad (144)$$

$$f_\theta(\mathbf{x}) = \frac{\sigma_v}{\sqrt{n}} \mathbf{v}^\top \mathbf{h}^{(T)}(\mathbf{x}) \quad (145)$$

Where we use new weights at each time step and we index it by time. Like previous sections, we first derive the forward pass kernels for two same length data $\mathbf{x} = \{\mathbf{x}_t\}_{t=1}^T, \mathbf{x}' = \{\mathbf{x}'_{t'}\}_{t'=1}^T$

$$\Sigma^{(t,t)}(\mathbf{x}, \mathbf{x}') = \sigma_w^2 \text{V}_\phi[\mathbf{K}^{(t,t)}(\mathbf{x}, \mathbf{x}')] + \frac{\sigma_u^2}{m} \langle \mathbf{x}_t, \mathbf{x}'_t \rangle + \sigma_b^2. \quad (146)$$

$$\Sigma^{(t,t')}(\mathbf{x}, \mathbf{x}') = 0 \quad t \neq t' \quad (147)$$

Since we are using same weight at the same time step, $\Sigma^{(t,t)}(\mathbf{x}, \mathbf{x}')$ can be written as a function of the previous kernel, which is exactly as the weight-tied RNN. However for different length, it becomes zero as a consequence of using different weights, unlike weight-tied which has non-zero value. The kernel of the first time step and output is also the same as weight-tied RNN. For the gradients we have:

$$\boldsymbol{\delta}^{(T)}(\mathbf{x}) = \sigma_v \mathbf{v} \odot \phi'(\mathbf{g}^{(T)}(\mathbf{x})) \quad (148)$$

$$\boldsymbol{\delta}^{(t)}(\mathbf{x}) = \frac{\sigma_w}{\sqrt{n}} (\mathbf{W}^{(t+1)})^\top \left(\phi'(\mathbf{g}^{(t)}(\mathbf{x})) \odot \boldsymbol{\delta}^{(t+1)}(\mathbf{x}) \right) \quad t \in [T-1] \quad (149)$$

For $t' = t$ we have:

$$\Pi^{(t,t)}(\mathbf{x}, \mathbf{x}') = \sigma_w^2 \mathbf{V}_{\phi'} [\mathbf{K}^{(t+1,t+1)}(\mathbf{x}, \mathbf{x}')] \Pi^{(t+1,t+1)}(\mathbf{x}, \mathbf{x}') \quad (150)$$

$$\Pi^{(t,t)}(\mathbf{x}, \mathbf{x}') = \sigma_v^2 \mathbf{V}_{\phi'} [\mathbf{K}^{(T+1,T+\tau+1)}(\mathbf{x}, \mathbf{x}')]. \quad (151)$$

Due to using different weights for $t \neq t'$, we can immediately conclude that $\Pi^{(t,t')}(\mathbf{x}, \mathbf{x}') = 0$. This set of calculation is exactly the same as the weight-tied case when $\tau = T - T = 0$.

Finally, with $\theta = \text{Vect}[\{\{\mathbf{W}^{(t)}, \mathbf{U}^{(t)}, \mathbf{b}^{(t)}\}_{t=1}^T, \mathbf{v}\}]$ we have

$$\langle \nabla_{\theta} f_{\theta}(\mathbf{x}), \nabla_{\theta} f_{\theta}(\mathbf{x}') \rangle = \sum_{t=1}^T \left\langle \frac{\partial f_{\theta}(\mathbf{x})}{\partial \mathbf{W}^{(t)}}, \frac{\partial f_{\theta}(\mathbf{x}')}{\partial \mathbf{W}^{(t)}} \right\rangle + \sum_{t=1}^T \left\langle \frac{\partial f_{\theta}(\mathbf{x})}{\partial \mathbf{U}^{(t)}}, \frac{\partial f_{\theta}(\mathbf{x}')}{\partial \mathbf{U}^{(t)}} \right\rangle \quad (152)$$

$$+ \sum_{t=1}^T \left\langle \frac{\partial f_{\theta}(\mathbf{x})}{\partial \mathbf{b}^{(t)}}, \frac{\partial f_{\theta}(\mathbf{x}')}{\partial \mathbf{b}^{(t)}} \right\rangle + \left\langle \frac{\partial f_{\theta}(\mathbf{x})}{\partial \mathbf{v}}, \frac{\partial f_{\theta}(\mathbf{x}')}{\partial \mathbf{v}} \right\rangle \quad (153)$$

with

$$\left\langle \frac{\partial f_{\theta}(\mathbf{x})}{\partial \mathbf{W}^{(t)}}, \frac{\partial f_{\theta}(\mathbf{x}')}{\partial \mathbf{W}^{(t)}} \right\rangle = \left(\frac{1}{n} \langle \delta^{(t)}(\mathbf{x}), \delta^{(t)}(\mathbf{x}') \rangle \right) \cdot \left(\frac{\sigma_w^2}{n} \langle \mathbf{h}^{(t-1)}(\mathbf{x}), \mathbf{h}^{(t-1)}(\mathbf{x}') \rangle \right) \quad (154)$$

$$\left\langle \frac{\partial f_{\theta}(\mathbf{x})}{\partial \mathbf{U}^{(t)}}, \frac{\partial f_{\theta}(\mathbf{x}')}{\partial \mathbf{U}^{(t)}} \right\rangle = \left(\frac{1}{n} \langle \delta^{(t)}(\mathbf{x}), \delta^{(t)}(\mathbf{x}') \rangle \right) \cdot \left(\frac{\sigma_u^2}{m} \langle \mathbf{x}_t, \mathbf{x}'_t \rangle \right) \quad (155)$$

$$\left\langle \frac{\partial f_{\theta}(\mathbf{x})}{\partial \mathbf{b}^{(t)}}, \frac{\partial f_{\theta}(\mathbf{x}')}{\partial \mathbf{b}^{(t)}} \right\rangle = \left(\frac{1}{n} \langle \delta^{(t)}(\mathbf{x}), \delta^{(t)}(\mathbf{x}') \rangle \right) \cdot \sigma_b^2 \quad (156)$$

$$\left\langle \frac{\partial f_{\theta}(\mathbf{x})}{\partial \mathbf{v}}, \frac{\partial f_{\theta}(\mathbf{x}')}{\partial \mathbf{v}} \right\rangle = \left(\frac{\sigma_v^2}{n} \langle \mathbf{h}^{(T)}(\mathbf{x}), \mathbf{h}^{(T)}(\mathbf{x}') \rangle \right). \quad (157)$$

As a result we obtain

$$\langle \nabla_{\theta} f_{\theta}(\mathbf{x}), \nabla_{\theta} f_{\theta}(\mathbf{x}') \rangle = \left(\sum_{t=1}^T \Pi^{(t,t)}(\mathbf{x}, \mathbf{x}') \cdot \Sigma^{(t,t)}(\mathbf{x}', \mathbf{x}') \right) + \mathcal{K}(\mathbf{x}, \mathbf{x}'), \quad (158)$$

same as the weight-tied RNN when $\tau = 0$. This concludes the proof for Theorem 3.

B.5 Analytical Formula for $\mathbf{V}_{\phi}[\mathbf{K}]$

For any positive definite matrix $\mathbf{K} = \begin{bmatrix} K_1 & K_3 \\ K_3 & K_2 \end{bmatrix}$ we have:

- $\phi = \text{ReLU}$

$$\mathbf{V}_{\phi}[\mathbf{K}] = \frac{1}{2\pi} \left(c(\pi - \arccos(c)) + \sqrt{1 - c^2} \right) \sqrt{K_1 K_2}, \quad (159)$$

$$\mathbf{V}_{\phi'}[\mathbf{K}] = \frac{1}{\pi} (\pi - \arccos(c)). \quad (160)$$

where $c = K_3 / \sqrt{K_1 K_2}$

- $\phi = \text{erf}$

$$\mathbf{V}_{\phi}[\mathbf{K}] = \frac{2}{\pi} \arcsin \left(\frac{2K_3}{\sqrt{(1+2K_1)(1+2K_3)}} \right), \quad (161)$$

$$\mathbf{V}_{\phi'}[\mathbf{K}] = \frac{4}{\pi \sqrt{(1+2K_1)(1+2K_2) - 4K_3^2}}. \quad (162)$$

C Proof for Theorem 2: RNTK Convergence after Training

To prove theorem 2, we use the strategy used in [27] which relies on the the local lipschitzness of the network Jacobian $\mathbf{J}(\theta, \mathcal{X}) = \nabla_{\theta} f_{\theta}(\mathbf{x}) \in \mathbb{R}^{|\mathcal{X}|^d \times |\theta|}$ at initialization.

Definition 1 *The Jacobian of a neural network is local lipschitz at NTK initialization ($\theta_0 \sim \mathcal{N}(0, 1)$) if there is constant $K > 0$ for every C such that*

$$\begin{cases} \|\mathbf{J}(\theta, \mathcal{X})\|_F < K \\ \|\mathbf{J}(\theta, \mathcal{X}) - \mathbf{J}(\tilde{\theta}, \mathcal{X})\|_F < K \|\theta - \tilde{\theta}\| \end{cases}, \quad \forall \theta, \tilde{\theta} \in B(\theta_0, R) \quad (163)$$

where

$$B(\theta, R) := \{\theta : \|\theta_0 - \theta\| < R\}. \quad (164)$$

Theorem 4 Assume that the network Jacobian is local lipschitz with high probability and the empirical NTK of the network converges in probability at initialization and it is positive definite over the input set. For $\epsilon > 0$, there exists N such that for $n > N$ when applying gradient flow with $\eta < 2(\lambda_{\min}(\Theta(\mathcal{X}, \mathcal{X})) + \lambda_{\max}(\Theta(\mathcal{X}, \mathcal{X})))^{-1}$ with probability at least $(1 - \epsilon)$ we have:

$$\sup_s \|\widehat{\Theta}_s(\mathcal{X}, \mathcal{X}) - \widehat{\Theta}_0(\mathcal{X}, \mathcal{X})\| = \mathcal{O}\left(\frac{1}{\sqrt{n}}\right). \quad (165)$$

Proof: See [27]

Theorem 4 holds for any network architecture and any cost function and it was used in [27] to show the stability of NTK for MLP during training.

Here we extend the results for RNTK by proving that the Jacobian of a multi-layer RNN under NTK initialization is local lipschitz with high probability.

To prove it, first, we prove that for any two points $\theta, \tilde{\theta} \in B(\theta_0, R)$ there exists constant K_1 such that

$$\|\mathbf{g}^{(\ell, t)}(\mathbf{x})\|_2, \|\delta^{(\ell, t)}(\mathbf{x})\|_2 \leq K_1 \sqrt{n} \quad (166)$$

$$\|\mathbf{g}^{(\ell, t)}(\mathbf{x}) - \tilde{\mathbf{g}}^{(\ell, t)}(\mathbf{x})\|_2, \|\delta^{(\ell, t)}(\mathbf{x}) - \tilde{\delta}^{(\ell, t)}(\mathbf{x})\|_2 \leq \|\bar{\theta} - \tilde{\theta}\| \leq K_1 \sqrt{n} \|\theta - \tilde{\theta}\|. \quad (167)$$

To prove 166 and 167 we use the following lemmas.³

Lemma 1 Let $A \in \mathbb{R}^{n \times m}$ be a random matrix whose entries are independent standard normal random variables. Then for every $t \geq 0$, with probability at least $1 - e^{-ct^2}$ for some constant c we have:

$$\|A\|_2 \leq \sqrt{m} + \sqrt{n} + t. \quad (168)$$

Lemma 2 Let $a \in \mathbb{R}^n$ be a random vector whose entries are independent standard normal random variables. Then for every $t \geq 0$, with probability at least $1 - e^{-ct^2}$ for some constant c we have:

$$\|a\|_2 \leq \sqrt{n} + \sqrt{t}. \quad (169)$$

Setting $t = \sqrt{n}$ for any $\theta \in R(\theta_0, R)$. With high probability, we get:

$$\|\mathbf{W}^{(\ell)}\|_2, \|\mathbf{U}^{(\ell)}\|_2 \leq 3\sqrt{n}, \quad \|\mathbf{b}^\ell\|_2 \leq 2\sqrt{n}, \quad \|\mathbf{h}^{(\ell, 0)}(\mathbf{x})\|_2 \leq 2\sigma_h \sqrt{n}. \quad (170)$$

We also assume that there exists some finite constant C such that

$$|\phi(x)| < C|x|, \quad |\phi(x) - \phi(x')| < C|x - x'|, \quad |\phi'(x)| < C, \quad |\phi'(x) - \phi'(x')| < C|x - x'|. \quad (171)$$

The proof is obtained by induction. From now on assume that all inequalities in 166 and 167 holds with some k for the previous layers. We have

$$\|\mathbf{g}^{(\ell, t)}(\mathbf{x})\|_2 = \left\| \frac{\sigma_w^\ell}{\sqrt{n}} \mathbf{W}^{(\ell)} \mathbf{h}^{(\ell, t-1)}(\mathbf{x}) + \frac{\sigma_u^\ell}{\sqrt{n}} \mathbf{U}^{(\ell)} \mathbf{h}^{(\ell-1, t)}(\mathbf{x}) + \sigma_b^\ell \mathbf{b}^{(\ell)} \right\|_2 \quad (172)$$

$$\leq \frac{\sigma_w^\ell}{\sqrt{n}} \|\mathbf{W}^{(\ell)}\|_2 \|\phi(\mathbf{g}^{(\ell, t-1)}(\mathbf{x}))\|_2 + \frac{\sigma_u^\ell}{\sqrt{n}} \|\mathbf{U}^{(\ell)}\|_2 \|\phi(\mathbf{g}^{(\ell-1, t)}(\mathbf{x}))\|_2 + \sigma_b^\ell \|\mathbf{b}^{(\ell)}\|_2 \quad (173)$$

$$\leq (3\sigma_w^\ell Ck + 3\sigma_u^\ell Ck + 2\sigma_b^\ell) \sqrt{n}. \quad (174)$$

And the proof for 166 and 167 is completed by showing that the first layer is bounded

$$\|\mathbf{g}^{(1, 1)}(\mathbf{x})\|_2 = \left\| \frac{\sigma_w^1}{\sqrt{n}} \mathbf{W}^{(1)} \mathbf{h}^{(1, 0)}(\mathbf{x}) + \frac{\sigma_u^1}{\sqrt{m}} \mathbf{U}^{(1)} \mathbf{x}_1 + \sigma_b^1 \mathbf{b}^{(1)} \right\|_2 \quad (175)$$

$$\leq (3\sigma_w^1 \sigma_h + \frac{3\sigma_u^1}{\sqrt{m}} \|\mathbf{x}_1\|_2 + 2\sigma_b^1) \sqrt{n}. \quad (176)$$

For the gradient of first layer we have

$$\|\delta^{(L, T)}(\mathbf{x})\|_2 = \|\sigma_v \mathbf{v} \odot \phi'(\mathbf{g}^{(L, T)}(\mathbf{x}))\|_2 \quad (177)$$

$$\leq \sigma_v \|\mathbf{v}\|_2 \|\phi'(\mathbf{g}^{(L, T)}(\mathbf{x}))\|_\infty \quad (178)$$

$$= 2\sigma_v C \sqrt{n}. \quad (179)$$

³See math.uci.edu/~rvershyn/papers/HDP-book/HDP-book.pdf for proofs

And similarly we have

$$\|\boldsymbol{\delta}^{(\ell,t)}(\mathbf{x})\| \leq (3\sigma_w Ck' + 3\sigma_u Ck') \sqrt{n}. \quad (180)$$

For $\theta, \tilde{\theta} \in B(\theta_0, R)$ we have

$$\|\mathbf{g}^{(1,1)}(\mathbf{x}) - \tilde{\mathbf{g}}^{(1,1)}(\mathbf{x})\|_2 = \left\| \frac{\sigma_w^1}{\sqrt{n}} (\mathbf{W}^{(1)} - \tilde{\mathbf{W}}^{(1)}) \mathbf{h}^{(1,0)}(\mathbf{x}) + \frac{\sigma_u^1}{\sqrt{m}} (\mathbf{U}^{(1)} - \tilde{\mathbf{U}}^{(1)}) \mathbf{h}^{(1,0)}(\mathbf{x}) \right\|_2 \quad (181)$$

$$\leq \left(3\sigma_w^1 \sigma_h + \frac{3\sigma_u^1}{m} \|\mathbf{x}_1\|_2 \right) \|\theta - \tilde{\theta}\|_2 \sqrt{n}. \quad (182)$$

$$\|\mathbf{g}^{(\ell,t)}(\mathbf{x}) - \tilde{\mathbf{g}}^{(\ell,t)}(\mathbf{x})\|_2 \leq \|\phi(\mathbf{g}^{(\ell,t-1)}(\mathbf{x}))\|_2 \left\| \frac{\sigma_w^\ell}{\sqrt{n}} (\mathbf{W}^{(\ell)} - \tilde{\mathbf{W}}^{(\ell)}) \right\|_2 \quad (183)$$

$$+ \left\| \frac{\sigma_w^\ell}{\sqrt{n}} \tilde{\mathbf{W}}^{(\ell)} \right\|_2 \|\phi(\mathbf{g}^{(\ell,t-1)}(\mathbf{x})) - \phi(\tilde{\mathbf{g}}^{(\ell,t-1)}(\mathbf{x}))\|_2 \quad (184)$$

$$+ \|\phi(\mathbf{g}^{(\ell-1,t)}(\mathbf{x}))\|_2 \left\| \frac{\sigma_u^\ell}{\sqrt{n}} (\mathbf{U}^{(\ell)} - \tilde{\mathbf{U}}^{(\ell)}) \right\|_2 \quad (185)$$

$$+ \left\| \frac{\sigma_u^\ell}{\sqrt{n}} \tilde{\mathbf{U}}^{(\ell)} \right\|_2 \|\phi(\mathbf{g}^{(\ell-1,t)}(\mathbf{x})) - \phi(\tilde{\mathbf{g}}^{(\ell-1,t)}(\mathbf{x}))\|_2 + \sigma_b \|\mathbf{b}^{(\ell)} - \tilde{\mathbf{b}}^{(\ell)}\| \quad (186)$$

$$\leq (k\sigma_w^\ell + 3\sigma_w^\ell Ck + k\sigma_u^\ell + 3\sigma_u^\ell Ck + \sigma_b) \|\theta - \tilde{\theta}\|_2 \sqrt{n}. \quad (187)$$

For gradients we have

$$\|\boldsymbol{\delta}^{(L,T)}(\mathbf{x}) - \tilde{\boldsymbol{\delta}}^{(L,T)}(\mathbf{x})\|_2 \leq \sigma_v \|\phi'(\mathbf{g}^{(L,T)}(\mathbf{x}))\|_\infty \|\mathbf{v} - \tilde{\mathbf{v}}\|_2 + \sigma_v \|\mathbf{v}\|_2 \|\phi'(\mathbf{g}^{(L,T)}(\mathbf{x})) - \phi'(\tilde{\mathbf{g}}^{(L,T)}(\mathbf{x}))\|_2 \quad (188)$$

$$\leq (\sigma_v C + 2\sigma_v Ck) \|\theta - \tilde{\theta}\|_2 \sqrt{n}. \quad (189)$$

And similarly using same techniques we have

$$\|\boldsymbol{\delta}^{(\ell,t)}(\mathbf{x}) - \tilde{\boldsymbol{\delta}}^{(\ell,t)}(\mathbf{x})\|_2 \leq (\sigma_w C + 3\sigma_w Ck + \sigma_u C + 3\sigma_u Ck) \|\theta - \tilde{\theta}\|_2 \sqrt{n}. \quad (190)$$

As a result, there exists K_1 that is a function of $\sigma_w, \sigma_u, \sigma_b, L, T$ and the norm of the inputs.

Now we prove the local Lipchitzness of the Jacobian

$$\|\mathbf{J}(\theta, \mathbf{x})\|_F \leq \sum_{\ell=2}^L \sum_{t=1}^T \left(\frac{1}{n} \left\| \boldsymbol{\delta}^{(\ell,t)}(\mathbf{x}) \left(\sigma_w^\ell \mathbf{h}^{(\ell,t-1)}(\mathbf{x}) \right)^\top \right\|_F \right) \quad (191)$$

$$+ \frac{1}{n} \left\| \boldsymbol{\delta}^{(\ell,t)}(\mathbf{x}) \left(\sigma_u^\ell \mathbf{h}^{(\ell,t-1)}(\mathbf{x}) \right)^\top \right\|_F + \frac{1}{\sqrt{n}} \left\| \boldsymbol{\delta}^{(\ell,t)}(\mathbf{x}) \cdot \sigma_b^\ell \right\|_F \quad (192)$$

$$+ \sum_{t=1}^T \left(\frac{1}{n} \left\| \boldsymbol{\delta}^{(1,t)}(\mathbf{x}) \left(\sigma_w^1 \mathbf{h}^{(1,t-1)}(\mathbf{x}) \right)^\top \right\|_F \right) \quad (193)$$

$$+ \frac{1}{\sqrt{nm}} \left\| \boldsymbol{\delta}^{(1,t-1)}(\mathbf{x}) \left(\sigma_u^1 \mathbf{x}_t \right)^\top \right\|_F + \frac{1}{\sqrt{n}} \left\| \boldsymbol{\delta}^{(1,t)}(\mathbf{x}) \cdot \sigma_b^1 \right\|_F + \frac{\sigma_v}{\sqrt{n}} \|\mathbf{h}^{(L,T)}(\mathbf{x})\|_F \quad (194)$$

$$\leq \left(\sum_{\ell=2}^L \sum_{t=1}^T (K_1^2 C \sigma_w^\ell + K_1^2 C \sigma_u^\ell + \sigma_b^\ell K_1) \right) \quad (195)$$

$$+ \sum_{t=1}^T \left(K_1^2 C \sigma_w^1 + \frac{K_1 \sigma_u^1}{\sqrt{m}} \|\mathbf{x}_t\|_2 + \sigma_b^1 K_1 \right) + \sigma_v C K_1. \quad (196)$$

And for $\theta, \tilde{\theta} \in B(\theta_0, R)$ we have

$$\|\mathbf{J}(\theta, \mathbf{x}) - \tilde{\mathbf{J}}(\theta, \mathbf{x})\|_F \leq \sum_{\ell=2}^L \sum_{t=1}^T \left(\frac{1}{n} \left\| \boldsymbol{\delta}^{(\ell,t)}(\mathbf{x}) \left(\sigma_w^\ell \mathbf{h}^{(\ell,t-1)}(\mathbf{x}) \right)^\top - \tilde{\boldsymbol{\delta}}^{(\ell,t)}(\mathbf{x}) \left(\sigma_w^\ell \tilde{\mathbf{h}}^{(\ell,t-1)}(\mathbf{x}) \right)^\top \right\|_F \right) \quad (197)$$

$$+ \frac{1}{n} \left\| \boldsymbol{\delta}^{(\ell,t)}(\mathbf{x}) \left(\sigma_u^\ell \mathbf{h}^{(\ell,t-1)}(\mathbf{x}) \right)^\top - \tilde{\boldsymbol{\delta}}^{(\ell,t)}(\mathbf{x}) \left(\sigma_u^\ell \tilde{\mathbf{h}}^{(\ell,t-1)}(\mathbf{x}) \right)^\top \right\|_F \quad (198)$$

$$+ \frac{1}{\sqrt{n}} \left\| \boldsymbol{\delta}^{(\ell,t)}(\mathbf{x}) \cdot \sigma_b^\ell - \tilde{\boldsymbol{\delta}}^{(\ell,t)}(\mathbf{x}) \cdot \sigma_b^\ell \right\|_F \quad (199)$$

$$+ \sum_{t=1}^T \left(\frac{1}{n} \left\| \boldsymbol{\delta}^{(1,t)}(\mathbf{x}) \left(\sigma_w^1 \mathbf{h}^{(1,t-1)}(\mathbf{x}) \right)^\top - \tilde{\boldsymbol{\delta}}^{(1,t)}(\mathbf{x}) \left(\sigma_w^1 \tilde{\mathbf{h}}^{(1,t-1)}(\mathbf{x}) \right)^\top \right\|_F \right) \quad (200)$$

$$+ \frac{1}{\sqrt{nm}} \left\| \boldsymbol{\delta}^{(1,t-1)}(\mathbf{x}) \left(\sigma_u^1 \mathbf{x}_t \right)^\top - \tilde{\boldsymbol{\delta}}^{(1,t-1)}(\mathbf{x}) \left(\sigma_u^1 \mathbf{x}_t \right)^\top \right\|_F \quad (201)$$

$$+ \frac{1}{\sqrt{n}} \left\| \boldsymbol{\delta}^{(\ell,t)}(\mathbf{x}) \cdot \sigma_b^\ell - \tilde{\boldsymbol{\delta}}^{(\ell,t)}(\mathbf{x}) \cdot \sigma_b^\ell \right\| + \frac{\sigma_v}{\sqrt{n}} \|\mathbf{h}^{(L,T)}(\mathbf{x}) - \mathbf{h}^{(L,\tilde{T})}(\mathbf{x})\|_F \quad (202)$$

$$\leq \left(\sum_{\ell=2}^L \sum_{t=1}^T (4K_1^2 C \sigma_w^\ell + 4K_1^2 C \sigma_u^\ell + \sigma_b^\ell K_1) \right) \quad (203)$$

$$+ \sum_{t=1}^T \left(4K_1^2 C \sigma_w^1 + \frac{K_1 \sigma_u^1}{\sqrt{m}} \|\mathbf{x}_t\|_2 + \sigma_b^1 K_1 \right) + \sigma_v C K_1 \|\theta - \tilde{\theta}\|_2. \quad (204)$$

The above proof can be generalized to the entire dataset by a straightforward application of the union bound. This concludes the proof for Theorem 2.